Inorganic Chemistry

FORUM ARTICLE

pubs.acs.org/IC

Ennobling an Old Molecule: Thiazyl Trifluoride ($N{\equiv}SF_3$), a Versatile Synthon for Xe−N Bond Formation

Gregory L. Smith, Hélène P. A. Mercier, and Gary J. Schrobilgen*

Department of Chemistry, McMaster University, Hamilton, Ontario L8S 4M1, Canada

Supporting Information

ABSTRACT: The fields of sulfur-nitrogen-fluorine chemistry and noble-gas chemistry have been significantly extended by the syntheses and characterizations of four new Xe−N-bonded cations derived from $N{\equiv}SF_3$. The adduct-cation, $F_3S{\equiv}NXeF^+$, has provided the entry point to a significant chemistry through HF solvolysis of the coordinated $N{\equiv}SF_3$ ligand and HF-catalyzed and solid-state rearrangements of $F_3S{\equiv}NXeF^+$. The HF solvolyses of $[F_3S{\equiv}NXeF][AsF_6]$ in anhydrous HF (aHF) and aHF/BrF_5 solutions yield the $F_4S{=}NXe^+$ cation, which likely arises from an HF-catalyzed mechanism. The $F_4S{=}NXe^+$ cation, in turn, undergoes HF displacement to form $F_4S{=}NH_2^+$ and XeF_2, as well as HF addition to the S=N bond to form $F_5SN(H)Xe^+$. Both cations undergo further solvolyses in aHF to form the $F_5SNH_3^+$ cation. The $F_4S{=}NXe^+$ and $F_4S{=}NH_2^+$ cations were characterized by NMR spectroscopy and single-crystal X-ray diffraction and exhibit high barriers to rotation about their S=N double bonds. They are the first cations known to contain the $F_4S{=}N-$ group and significantly extend the chemistry of this ligand. The solid-state rearrangement of $[F_3S{\equiv}NXeF][AsF_6]$ at 22 °C has yielded $[F_4S{=}NXe][AsF_6]$, which was characterized by Raman spectroscopy, providing the first examples of xenon bonded to an imido nitrogen and of the $F_4S{=}N-$ group bonded to a noble-gas element. The rearrangement of $[F_3S{\equiv}NXeF][AsF_6]$ in a $N{\equiv}SF_3$ solution at 0 °C also yielded $[F_4S{=}NXe{-}N{\equiv}SF_3][AsF_6]$, which represents a rare example of a N−Xe−N linkage and the first to be characterized by X-ray crystallography. Solvolysis of $N{\equiv}SF_3$ in aHF was previously shown to give the primary amine F_5SNH_2, whereas solvolysis in the superacid medium, AsF_5/aHF, results in amine protonation to give $[F_5SNH_3][AsF_6]$. Complete structural characterizations were not available for either species. Isolation of $F_5SNH_2 \cdot n$HF from the reaction of $N{\equiv}SF_3$ with HF has provided a structural characterization of F_5SNH_2 by Raman spectroscopy. Crystal growth by sublimation of $F_5SNH_2 \cdot n$HF at −30 to −40 °C has resulted in the X-ray crystal structure of $F_5SNH_2 \cdot 2[F_5SNH_3][HF_2] \cdot 4$HF and structural characterizations of F_5SNH_2 and $F_5SNH_3^+$. The redox decomposition of $[F_4S{=}NXe{-}N{\equiv}SF_3][AsF_6]$ in $N{\equiv}SF_3$ at 0 °C generated Xe, *cis*-N_2F_2, and $[F_3S(N{\equiv}SF_3)_2][AsF_6]$.

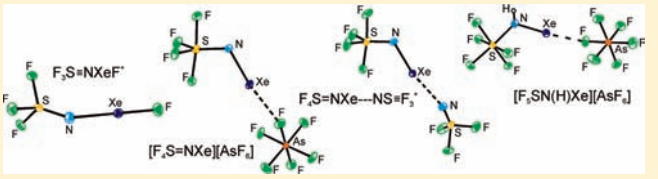

INTRODUCTION

Thiazyl trifluoride, $N{\equiv}SF_3$, is among the first reported compounds containing only sulfur, nitrogen, and fluorine.[1,2] Over the 56 years that have elapsed since its discovery, the field of sulfur-nitrogen-fluorine chemistry has grown significantly, and several reviews have been written on the topic;[3−6] however, a recent comprehensive review of the topic is unavailable. The present Article focuses on the most recent developments in $N{\equiv}SF_3$ chemistry and their impacts on noble-gas chemistry. Those aspects of $N{\equiv}SF_3$ reactivity that are most pertinent to the present Article are briefly commented upon and illustrated in the following overview and are by no means representative of the breadth of the field.

Thiazyl trifluoride is usually prepared by a three-step procedure that requires $Si(NCO)_4$ as the precursor. Tetraisocyanatosilane is prepared by the reaction of $SiCl_4$ with KOCN in SO_2 solvent.[7] The reaction of $Si(NCO)_4$ with SF_4 produces $FC(O)N{=}SF_2$,[8] which is oxidatively fluorinated by AgF_2 to give $N{\equiv}SF_3$.[9] Unlike N≡SF, $N{\equiv}SF_3$ (mp −72.6 °C; bp −27.1 °C)[10] is kinetically very stable, resisting hydrolysis by weak acids, and does not react with sodium metal below ca. 200 °C,[5,10] resembling SF_6 in its resistance to nucleophilic attack.

The geometry of $N{\equiv}SF_3$ is well established, having been determined by ^{19}F NMR,[11] IR,[10−12] Raman,[13] and microwave spectroscopy[14] and most recently by single-crystal X-ray diffraction.[15,16] Like isoelectronic SO_2F_2, $N{\equiv}SF_3$ has a distorted tetrahedral geometry (Figure 1), with a formal N≡S triple bond and an electron lone pair on nitrogen.

In general, and in the context of this Article, the reactivity of $N{\equiv}SF_3$ mainly embraces three areas:[5] (1) reactions with electrophiles that occur by donation of the electron lone pair on nitrogen to a Lewis acid center, (2) addition reactions involving the π system of the N≡S triple bond, and (3) nucleophilic reactions that occur at the positively charged and coordinatively unsaturated sulfur atom.

The stability of $N{\equiv}SF_3$ toward the strong Lewis acid oxidants AsF_5 and SbF_5 has resulted in the Lewis acid-base adducts $F_3S{\equiv}NAsF_5$[17] and $F_3S{\equiv}NSbF_5$,[17] as well as $F_3S{\equiv}NBF_3$ when reacted with the much weaker Lewis acid BF_3.[10,18] Thiazyl trifluoride is also sufficiently basic to function as a main-group

Received: May 30, 2011
Published: July 27, 2011

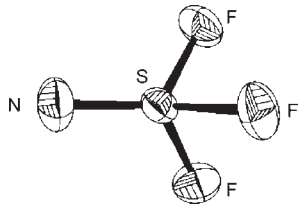

Figure 1. X-ray crystal structure of $N{\equiv}SF_3$. Thermal ellipsoids are shown at the 50% probability level. Bond lengths (Å): S(1)−N(1), 1.400(3); S(1)−F(1), 1.5309(4); S(1)−F(2), 1.534(2). Bond angles (deg): N(1)−S(1)−F(1), 122.44(9); N(1)−S(1)−F(2), 121.76(16); F(1)−S(1)−F(2), 94.16(9); F(1)−S(1)−F(1A), 94.36(12). Reproduced with permission from ref 15.

and transition-metal element ligand, e.g., $[(CF_3)_nSF_{3-n}{\cdot}N{\equiv}SF_3][AsF_6]$[19] and $[M(N{\equiv}SF_3)_4][AsF_6]_2$ (M = Mn, Fe, Co, Ni, Cu).[20] Protonation of $N{\equiv}SF_3$ occurs in the superacidic medium HSO_3F/SbF_5 below −80 °C, but at higher temperatures, the equilibrium favors $F_3S{\equiv}NSbF_5$ and $HSO_3F{\cdot}N{\equiv}SF_3$ adduct formation.[5,21]

Although cations of the type $XN{\equiv}SF_3^+$ are likely the primary products in reactions that involve the addition of the polar reagents, XF (X = H, Cl), to the N≡S triple bond of $N{\equiv}SF_3$, neither has been isolated. Rather, the reactions of XF (X = H, Cl) with $N{\equiv}SF_3$ result in the addition of 2 equiv of XF across the N≡S bond, yielding F_5SNCl_2 and F_5SNH_2.[22,23] However, when alkyl groups [R = CH_3, C_2H_5, $(CH_3)_2CH$] are used to lower the electrophilicities of the cationic addition products, the $RN{\equiv}SF_3^+$ salts can be isolated.[24] Solvolysis of $N{\equiv}SF_3$ in the superacid medium, AsF_5/aHF, results in amine protonation to give $[F_5SNH_3][AsF_6]$.[25]

Localization of the electron density on the sulfur atom is enhanced by back-bonding from the fluorine atoms in $N{\equiv}SF_3$ and SF_6, making nucleophilic attack at sulfur more difficult. While there is no direct evidence that the nucleophilic addition of a fluoride ion to $N{\equiv}SF_3$ gives $N{=}SF_4^-$, reactions with F_2, in the presence of CsF, and with Cl_2, in the presence of HgF_2, give F_5SNF_2 and F_5SNCl_2, respectively, suggesting that the $N{=}SF_4^-$ anion is an intermediate.[5] Nucleophilic attack by OH^- at the sulfur atom of $N{\equiv}SF_3$ occurs when hot alkali is used, yielding $HN{=}SOF_2$ as the first hydrolysis product. Its presence was inferred by the precipitation of $[P(C_6H_5)_4][N{=}SOF_2]$, with subsequent hydrolyses leading to nonisolable H_2NSO_2F, H_2NSO_3H, and $[NH_4][HSO_4]$.[26] These and other nucleophilic substitution reactions with $N{\equiv}SF_3$ form the basis for a significant body of work in the field of sulfur-nitrogen-fluorine chemistry.[5,15,27] Products of nucleophilic substitution at sulfur that retain the formal N≡S triple bond are generated when $N{\equiv}SF_3$ reacts with secondary amines[28] or alcohols,[29] perfluoroalkylating reagents[30,31] or organolithium reagents.[32]

In recent years, a new role has emerged for $N{\equiv}SF_3$ as a synthon for Xe−N bond formation. Prior to the research highlighted in this Article, several xenon(II) species were known in which xenon is bonded to nitrogen having formal sp, sp^2, or sp^3 hybridization. Most belong to a class of weakly bonded XeF^+ adducts with organic nitrogen bases. Those exhibiting formal nitrogen sp hybridization are represented by the XeF^+ adducts of hydrogen cyanide,[33,34] alkylnitriles,[33] pentafluorobenzenenitrile,[33] and perfluoroalkylnitriles.[33,35] Examples of XeF^+ adducts with sp^2-hybridized organic nitrogen bases were also known, namely, those with *s*-trifluorotriazine[35] and several perfluoropyridines.[36]

The only previously known example in which xenon was bonded to sp^3-hybridized nitrogen was $F_5TeN(H)Xe^+$.[37] The known Xe−N-bonded species bonded to sp^2-hybridized inorganic nitrogen ligands are those derived from the imidobis(fluorosulfonyl) group and include $FXeN(SO_2F)_2$,[38−40] $Xe[N(SO_2F)_2]_2$,[39,41] $F[XeN(SO_2F)_2]_2^+$,[39,41,42] and $XeN(SO_2F)_2^+$,[42] as well as the related imidobis(trifluoromethylsulfonyl) group, which is solely represented by $Xe[N(SO_2CF_3)_2]_2$.[43]

The research highlighted in this Article springs from $N{\equiv}SF_3$ and represents significant extensions of both the fields of sulfur-nitrogen-fluorine and noble-gas chemistry with the syntheses of four new Xe−N-bonded species, namely, $F_3S{\equiv}NXeF^+$, $F_4S{=}NXe^+$, $F_5SN(H)Xe^+$, and $F_4S{=}NXe{---}N{\equiv}SF_3^+$. This work has also led to the syntheses and characterizations of two new sulfur-nitrogen-fluorine cations, $F_4S{=}NH_2^+$ and $F_3S(N{\equiv}SF_3)_2^+$, as well as to fuller structural characterizations of F_5SNH_2 and $F_5SNH_3^+$.

SYNTHESES AND STRUCTURES OF Xe−N-BONDED AND RELATED CATIONS DERIVED FROM $N{\equiv}SF_3$

The reaction of oxidatively resistant $N{\equiv}SF_3$ (the first ionization potential obtained from the X-ray photoelectron spectrum of $N{\equiv}SF_3$ is 12.50 eV[44]) with the strongly electrophilic Lewis acid cation, XeF^+, providing the entry point for the syntheses of the xenon cations discussed in this Article. Their initial structural characterizations have been primarily carried out in anhydrous HF (aHF) solvent by ^{19}F and ^{129}Xe NMR spectroscopy.

I. $F_3S{\equiv}NXeF^+$ Cation, a Precursor for Xe−N Bond Formation. Liquid $N{\equiv}SF_3$, synthesized as previously described,[7−9] reacts with $[XeF][AsF_6]$ at −25 to −15 °C over a period of 6 h to form $[F_3S{\equiv}NXeF][AsF_6]$ (eq 1). The salt is colorless and

$$N{\equiv}SF_3 + [XeF][AsF_6] \xrightarrow[-25\ to\ -15\ ^\circ C]{N{\equiv}SF_3} [F_3S{\equiv}NXeF][AsF_6] \quad (1)$$

microcrystalline with a limited stability at room temperature and has been structurally characterized by solution multi-NMR spectroscopy, as well as in the solid state by Raman spectroscopy (−150 °C) and single-crystal X-ray diffraction[45] (see Solid-State Rearrangement of $[F_3S{\equiv}NXeF][AsF_6]$).

The $F_3S{\equiv}NXeF^+$ cation was characterized by ^{19}F, ^{129}Xe, and ^{14}N NMR spectroscopy in aHF (or BrF_5) solvent at −20 °C.[45] The ^{19}F NMR spectrum consists of two singlets at 51.2 (53.3) and −185.5 (−180.5) ppm, corresponding to the fluorine-on-sulfur (F-on-S) and fluorine-on-xenon (F-on-Xe) environments, respectively (Figure 2). The more shielded resonance is accompanied by natural abundance ^{129}Xe (26.44%) satellites resulting from $^1J(^{129}Xe-^{19}F)$ = 6265 (6248) Hz. The $^4J(^{19}F_{Xe}-^{19}F_S)$ coupling cannot be observed in HF solvent, which may be a consequence of line broadening (F-on-S, $\Delta\nu_{1/2}$ = 47 Hz; F-on-Xe, $\Delta\nu_{1/2}$ = 150 Hz) arising from slow chemical exchange between HF and F-on-Xe of $F_3S{\equiv}NXeF^+$. The $^4J(^{19}F_{Xe}-^{19}F_S)$ coupling (doublet, 15.1 Hz, $\Delta\nu_{1/2}$ = 26 Hz) is observed, however, in BrF_5 at −60 °C. The anticipated 1:3:3:1 quartet corresponding to the F-on-Xe environment could only be partially resolved in BrF_5 solvent ($\Delta\nu_{1/2}$ = 45 Hz).

The ^{129}Xe NMR spectrum (Figure 3) is comprised of a doublet arising from $^1J(^{129}Xe-^{19}F)$ = 6265 (6248) Hz, which, in turn, is split into a 1:1:1 triplet [$^1J(^{129}Xe-^{14}N)$ = 350 Hz] in aHF. The outer transitions of the triplets are broader than the central transition owing to partial quadrupolar relaxation of ^{14}N

dx.doi.org/10.1021/ic201161q |*Inorg. Chem.* 2011, 50, 12359–12373

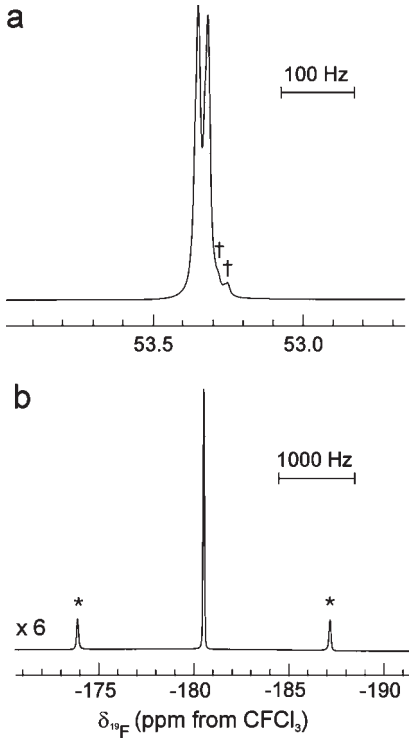

Figure 2. ^{19}F NMR spectrum (470.592 MHz) of $[F_3S{\equiv}NXeF][AsF_6]$ in BrF_5 solvent at −60 °C showing the cation resonances: (a) F-on-S environment. Daggers (†) denote the $^1\Delta^{19}F_S(^{34/32}S)$ secondary isotope shift. (b) F-on-Xe environment. Asterisks (*) denote ^{129}Xe satellites. Reproduced with permission from ref 45.

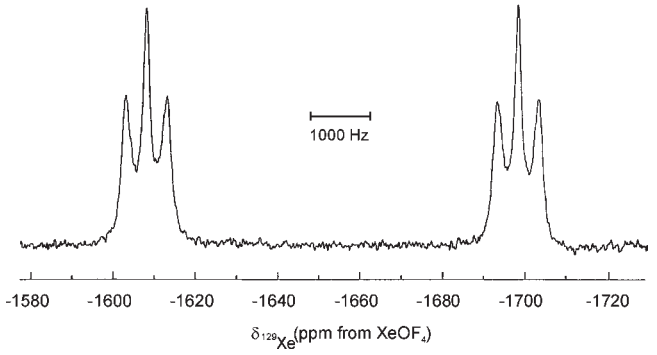

Figure 3. ^{129}Xe NMR spectrum (138.086 MHz) of $[F_3S{\equiv}NXeF][AsF_6]$ in aHF solvent at −20 °C. Reproduced with permission from ref 45.

($I = 1$) due to the small electric field gradient at ^{14}N in this axially symmetric cation.

Similar $^1J(^{129}Xe-^{14}N)$ couplings have been observed for the HC≡N and alkyl nitrile adducts of XeF^+ when recorded in HF solvent [cf. $HC{\equiv}NXeF^+$, $^1J(^{129}Xe-^{19}F)$ = 6161 Hz and $^1J(^{129}Xe-^{14}N)$ = 332 Hz at −10 °C[34]. The ^{129}Xe NMR chemical shift, $\delta(^{129}Xe)$ = −1652 (−1661) ppm, is consistent with that expected for XeF^+ coordinated to sp-hybridized nitrogen [cf. $HC{\equiv}NXeF^+$, $\delta(^{129}Xe)$ = 1552 (−1570) ppm in aHF (BrF_5) solvent at −10 (−50) °C[34]. In BrF_5 solvent, the $^1J(^{129}Xe-^{14}N)$ coupling of $F_3S{\equiv}NXeF^+$ was quadrupole-collapsed to a doublet corresponding to $^1J(^{129}Xe-^{19}F)$. The ^{14}N NMR spectrum in HF is a quadrupole broadened singlet at −278.0 ppm (−20 °C) in which the ^{129}Xe satellites are unresolved.

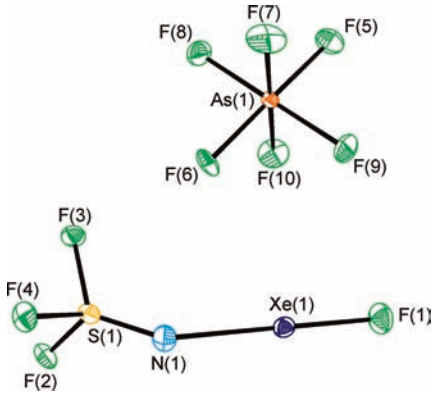

Figure 4. Structural unit in the X-ray crystal structure of $[F_3S{\equiv}NXe][AsF_6]$. The thermal ellipsoids are shown at the 50% probability level. Bond lengths (Å): S(1)−N(1), 1.397(5); S(1)−F(2), 1.503(3); S(1)−F(3), 1.503(3); S(1)−F(4), 1.496(3); Xe(1)−N(1), 2.236(4); Xe(1)−F(1), 1.938(3). Bond angles (deg): Xe(1)−N(1)−S(1), 142.6(3); N(1)−Xe(1)−F(1), 179.6(2). Reproduced with permission from ref 45.

The X-ray crystal structure of $[F_3S{\equiv}NXeF][AsF_6]$ (Figure 4) is comprised of well-separated $F_3S{\equiv}NXeF^+$ cations and AsF_6^- anions showing no significant distortion from octahedral symmetry (cf. $[F_5TeNH_3][AsF_6]$[37] and $[Xe_2F_3][AsF_6]$[46]). The Xe(1)−N(1) and Xe(1)−F(1) bond lengths are equal, within experimental error, to those of $[HC{\equiv}NXeF][AsF_6]$ [2.235(3) and 1.936(2) Å][47] and are comparable to those observed in $[CH_3C{\equiv}NXeF][AsF_6]\cdot HF$ [2.179(7) and 1.947(5) Å][47] and $[(CH_3)_3CC{\equiv}NXeF][AsF_6]$ [2.212(4) and 1.952(3) Å].[47] The Xe(1)−F(1) bond of $F_3S{\equiv}NXeF^+$ is significantly longer than the terminal Xe−F bond in $[XeF][AsF_6]$ [1.873(6)[48] and 1.888(3)[49] Å] and other XeF^+ salts[49,50] but shorter than those in XeF_2 [1.999(4)[49] Å]. The relationship between the relative strengths of the donor-acceptor interactions in XeF^+ salts, i.e., $FXe^+{---}F{-}MF_5^-$ and $FXe^+{---}F{-}M_2F_{10}^-$ and the Xe−F bond length generally leads to Xe−F bond strengthening and to a corresponding increase in $\nu(XeF)$[49,51,52] with decreasing fluorobasicity of the fluoro anion. Among the crystallographically characterized N−Xe−F-bonded cations having formal sp hybridization at N, the Xe−N and Xe−F bond lengths in the $F_3S{\equiv}NXeF^+$ cation are most similar to those of $HC{\equiv}NXeF^+$[47] and to the terminal Xe−F bond lengths of $Xe_2F_3^+$ ($[Xe_2F_3][AsF_6]$, 1.915(8) Å),[46] placing the XeF^+ adducts of $N{\equiv}SF_3$ and $HC{\equiv}N$ toward the most ionic end of the scale.

The N(1)≡S(1) and S(1)−F bonds of $[F_3S{\equiv}NXeF][AsF_6]$ are significantly shorter than those in $N{\equiv}SF_3$.[14,15] Similar bond-length contractions occur in other $N{\equiv}SF_3$ complexes, e.g., $F_3S{\equiv}NAsF_5$ (1.383 and 1.439 Å, respectively),[5] $[Mn(N{\equiv}SF_3)_4][AsF_6]_2$ [av. 1.365(11) Å and av. 1.506(5) Å],[53] and $[CpFe(CO)_2N{\equiv}SF_3][AsF_6]$ [1.376(3) Å and av. 1.515(3) Å].[54] Such bond-length contractions have been rationalized in terms of the change in hybridization of the valence electron lone pair on the nitrogen atom that occurs upon adduct formation. The change from predominantly s to sp hybrid character upon coordination leads to strengthening and contraction of the S−N σ bond and removal of the charge density from the sulfur atom, resulting in shorter, more covalent S−F bonds, which has been attributed to enhanced S−F π back-bonding.[5,18] Negative $\pi_N \rightarrow \sigma^*_{SF}$ type hyperconjugation, which results in π_{SN} bonding, has been considered to be the primary contributor to π_{SN} bonding in

dx.doi.org/10.1021/ic201161q |Inorg. Chem. 2011, 50, 12359–12373

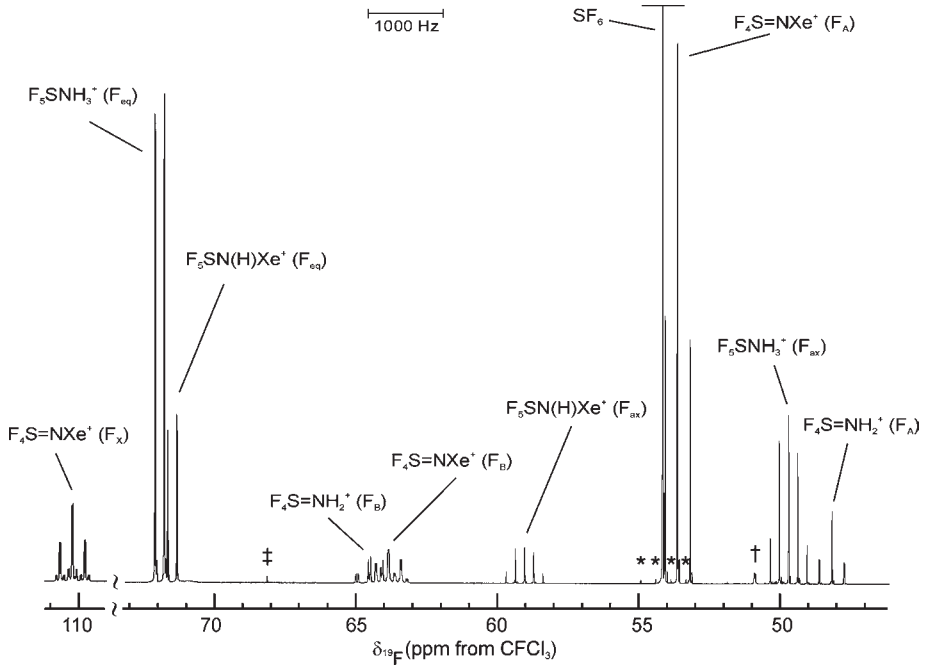

Figure 5. ^{19}F NMR spectrum (470.592 MHz) of the product mixture resulting from solvolysis of $[F_3S{\equiv}NXeF][AsF_6]$ for 30 min in aHF solvent at −20 °C. Symbols denote F-on-S of residual $F_3S{\equiv}NXeF^+$ (†), the 1:1:1:1 quartet arising from $^1J(^{19}F-^{33}S)$ of SF_6 (*), and a very weak unassigned resonance (‡). The XeF_2 resonance, not shown in the spectral trace, occurred at $\delta(^{19}F) = -194.5$ ppm with $^1J(^{19}F-^{129}Xe) = 5652$ Hz. Reproduced from ref 58.

$N{\equiv}SF_3$, with $\pi_N \rightarrow d_\pi(S)$ overlap being secondary.[55] In this model, the σ bonding is significantly ionic, with the strongly polar σ^*_{SN} orbitals serving as more effective electron acceptors than extravalence $d_\pi(S)$ orbitals.

The calculated natural bond orbital (NBO) charges, bond orders, and valencies [MP2/aug-cc-pVTZ(-PP)][56] are in accordance with the highly ionic natures of the σ frameworks in $N{\equiv}SF_3$ and $F_3S{\equiv}NXeF^+$, showing significant polarization of the N electron density upon coordination of the strong Lewis acid acceptor, XeF^+ (N charges; $N{\equiv}SF_3$, −0.81; $F_3S{\equiv}NXeF^+$, −1.10), and, in turn, serves to polarize S (charges; $N{\equiv}SF_3$, 2.18; $F_3S{\equiv}NXeF^+$, 2.47) and F_S (charges; $N{\equiv}SF_3$, −0.46; $F_3S{\equiv}NXeF^+$, −0.40). Corresponding increases in the S−F bond orders ($N{\equiv}SF_3$, 0.38; $F_3S{\equiv}NXeF^+$, 0.45) and F_S valencies ($N{\equiv}SF_3$, 0.30; $F_3S{\equiv}NXeF^+$, 0.33) also occur. Although the S−N bond length decreases upon coordination and the valencies of S ($N{\equiv}SF_3$, 2.33; $F_3S{\equiv}NXeF^+$, 2.44) and N ($N{\equiv}SF_3$, 1.01; $F_3S{\equiv}NXeF^+$, 1.23) increase, the total S−N bond order is little affected ($N{\equiv}SF_3$, 1.18; $F_3S{\equiv}NXeF^+$, 1.09).

Although quantum-chemical calculations predict a linear structure,[45] the Xe(1)−N(1)−S(1) angle deviates significantly from linearity, which likely results from several close N···F contacts within the crystal lattice, three from anions and one from the fluorine ligand bonded to xenon in a neighboring $F_3S{\equiv}NXeF^+$ cation. These contacts are at the limit of the sum of the nitrogen and fluorine van der Waals radii (3.02 Å),[57] and form a distorted square-planar arrangement about nitrogen, with the Xe−N−S angle bent toward the longest, most open edge.[45] The N−S−F and F−S−F angles in $[F_3S{\equiv}NXeF][AsF_6]$ average 119.8(2)° and 97.4(2)°, respectively, comprising a distorted tetrahedral arrangement about sulfur that is similar to those of $N{\equiv}SF_3$ [122.4(3) and 94.0(3)°;[14] 122.1(18) and 94.26(14)°], $F_3S{\equiv}NAsF_5$ (122.2 and 94.3°),[5] and $[CpFe(CO)_2N{\equiv}SF_3][AsF_6]$ [av. 120.9(4)° and av. 96.0(4)°].[54]

Scheme 1. Proposed HF-Catalyzed Solution Rearrangement of $F_3S{\equiv}NXeF^+$ Leading to $F_4S{=}NXe^+$ (Adapted from Reference 58)

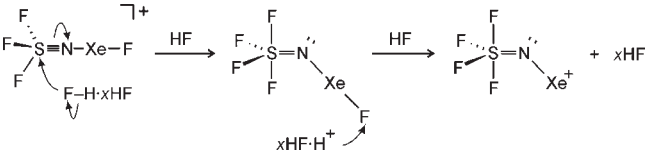

II. Solvolysis of $[F_3S{\equiv}NXeF][AsF_6]$ in aHF. Controlled solvolysis of $[F_3S{\equiv}NXeF][AsF_6]$ in aHF or aHF/BrF_5 at −20 to 0 °C yields a complex mixture of $F_4S{=}NXe^+$, $F_4S{=}NH_2^+$, $F_5SN(H)Xe^+$, and $F_5SNH_3^+$ cations. With careful temperature control, it has been possible to obtain the ^{19}F NMR spectra of the entire series of solvolysis products (Figure 5).[58] NMR assignments of individual species were confirmed by spectral simulation, which provided calculated NMR spectra that are in excellent agreement with the experimental ones.

(a) $F_4S{=}NXe^+$. The $F_4S{=}NXe^+$ cation was formed by the reaction of $[F_3S{\equiv}NXeF][AsF_6]$ with HF for ca. 1 h at −20 °C in aHF or HF/BrF_5 solution (eq 2). The reaction likely proceeds

$$F_3S{\equiv}NXeF^+ \xrightarrow[HF\ or\ HF/BrF_5]{-20\ ^\circ C} F_4S{=}NXe^+ \qquad (2)$$

through the two-step HF-catalyzed rearrangement shown in Scheme 1. The $F_4S{=}NXe^+$ cation was shown by ^{19}F and ^{129}Xe NMR spectroscopy to be a major component of the solvolysis product mixture. The proposed neutral imide, $F_4S{=}NXeF$, has neither been observed in situ nor has it been isolated.

dx.doi.org/10.1021/ic201161q |*Inorg. Chem.* 2011, 50, 12359–12373

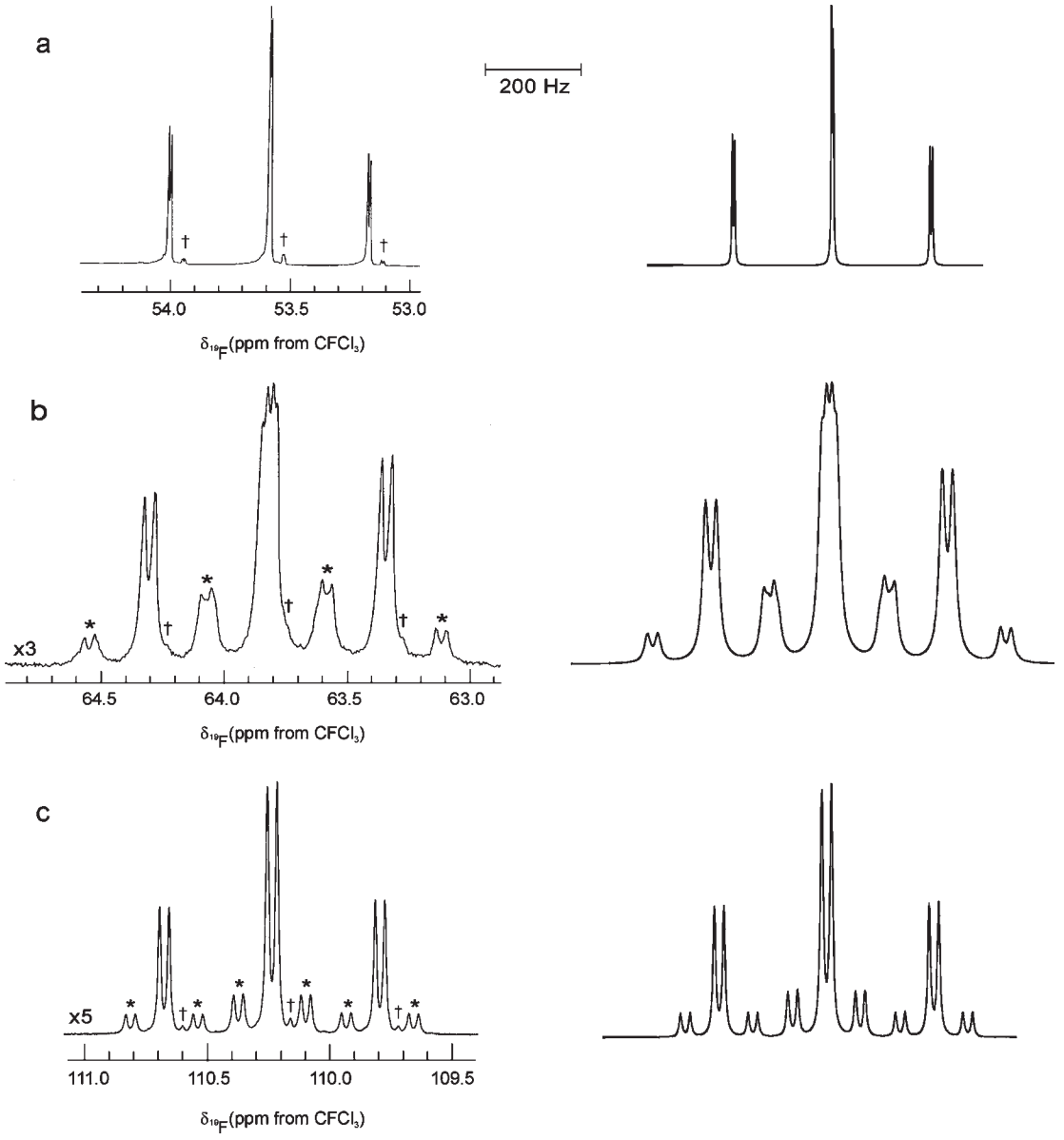

Figure 6. ^{19}F NMR spectrum (470.592 MHz) of $F_4S{=}NXe^+$ in HF solvent at −20 °C (left-hand traces) and simulated spectrum (right-hand traces) depicting (a) F_A, (b) F_B, and (c) F_X. Symbols denote the $^1\Delta^{19}F(^{34/32}S)$ secondary isotope shifts (†) and ^{129}Xe satellites (*) in the experimental spectrum. Reproduced from ref 58.

$A_2BX\Omega$

Structure I

The ^{19}F NMR spectrum of the $F_4S{=}NXe^+$ cation (Figure 6) is a superposition of the A_2BX spin-coupling pattern of the $F_4S{=}N-$ group and the $A_2BX\Omega$ satellite spectra (Structure I) resulting from coupling to natural abundance ^{129}Xe ($I = {}^1/_2$, 26.44%; indicated by Ω). Xenon-129 satellites are only observed on the axial B and X fluorine resonances. The pseudotriplet corresponding to the equatorial F_A environment of $F_4S{=}NXe^+$ is comprised of a doublet of doublets that results from the two near-equal couplings, $^2J(^{19}F_A{-}^{19}F_B)$ = 206.8 Hz and $^2J(^{19}F_A{-}^{19}F_X)$ = 206.5 Hz, which are similar to those of related species, e.g., $F_4S{=}NF$ (213.9 and 194.0 Hz),[59,60] $F_4S{=}NCH_3$ (201 and 194.0 Hz),[24] and $F_4S{=}NCF_2CF_3$ (208.0 and 210.6 Hz).[61] The F_B and F_X multiplets are each comprised of a doublet of triplets, with the triplets arising from $^2J(^{19}F_A{-}^{19}F_{B/X})$ (vide supra) and the doublets arising from $^2J(^{19}F_B{-}^{19}F_X)$ = 18.2 Hz. The multiplets are accompanied by natural abundance ^{129}Xe satellites resulting from $^3J(^{129}Xe{-}^{19}F_B)$ = 203.6 Hz and $^3J(^{129}Xe{-}^{19}F_X)$ = 129.7 Hz, respectively, with the satellites of the central peak of the F_B multiplet overlapping with the inner satellites of the outer multiplet lines. The additional fine structure that is manifested in the small unequal doublet splittings on each of the F_A triplet transitions, the additional transitions in the central peak of the F_B multiplet, and the broadening of the F_B

dx.doi.org/10.1021/ic201161q |Inorg. Chem. 2011, 50, 12359–12373

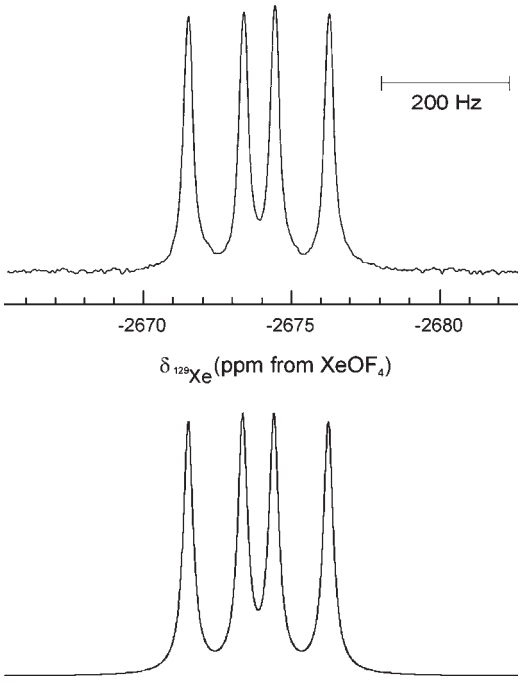

Figure 7. ^{129}Xe NMR spectrum (138.086 MHz) of $F_4S{=}NXe^+$ in HF solvent at −20 °C (upper trace) and simulated spectrum (lower trace). Reproduced from ref 58.

and, to a lesser extent, F_X resonances are due to second-order effects, which were confirmed by spectral simulation.

The ^{129}Xe NMR spectrum of $F_4S{=}NXe^+$ (Figure 7) is a doublet of doublets, resulting from $^3J(^{129}Xe{-}^{19}F_B)$ and $^3J(^{129}Xe{-}^{19}F_X)$ (vide supra), centered at −2674 ppm. No $^3J(^{129}Xe{-}^{19}F_A)$ coupling was observed (vide infra). The ^{129}Xe NMR chemical shift is consistent with that expected for xenon bound to a sp^2-hybridized nitrogen but is considerably more shielded than the ^{129}Xe resonances of $Xe[N(SO_2CF_3)_2]_2$ (−2444 ppm in SO_2ClF at 8 °C),[41] $Xe[N(SO_2F)_2]_2$ (−2257 ppm in SO_2ClF at −40 °C),[41] $FXeN(SO_2F)_2$ (−2009 ppm in SO_2ClF at −40 °C),[41] $XeN(SO_2F)_2^+$ (−1943 ppm in SbF_5 at 25 °C),[42] and $F[XeN(SO_2F)_2]_2^+$ (−1955 ppm in BrF_5 at −59 °C).[41] It is noteworthy that the $^3J(^{129}Xe{-}^{19}F_X)$ coupling in $N{\equiv}SF_3$ solvent (102.0 Hz) is significantly less than that in aHF or BrF_5 solvent (129.7 and 126.7 Hz, respectively), whereas the remaining coupling constants are very similar irrespective of the solvent. This is likely a consequence of weak coordination of $N{\equiv}SF_3$ solvent molecules to the xenon atom of the cation.

The $^3J(^{19}F_A{-}^{129}Xe)$ coupling could not be resolved in either the ^{19}F or ^{129}Xe NMR spectrum when recorded in aHF, BrF_5, or $N{\equiv}SF_3$ solvent. The small to near-zero value of this coupling may stem from a Karplus-type dependence,[62] where the absolute three-bond coupling constant is a minimum when the dihedral angle between the coupled nuclei is 90°. The minimum $^3J(^{19}F_A{-}^{129}Xe)$ coupling is achieved when the F$_A$−S−N−Xe dihedral angle is 90°. This is also consistent with the fluorine-fluorine coupling trend in $F_4S{=}NF$, for which the $^3J(^{19}F_N{-}^{19}F_A)$ coupling (F_N is F-on-N) is an order of magnitude smaller than $^3J(^{19}F_N{-}^{19}F_B)$ or $^3J(^{19}F_N{-}^{19}F_X)$.[59]

(b) $F_4S{=}NH_2^+$. The $F_4S{=}NH_2^+$ cation is formed, along with $F_4S{=}NXe^+$, during the solvolysis of $F_3S{\equiv}NXeF^+$ in aHF at −20 °C. The reaction of $F_4S{=}NXe^+$ with 2 equiv of HF resulted in $F_4S{=}NH_2^+$ and XeF_2 formation according to eq 3, which were identified by ^{19}F NMR spectroscopy.[58]

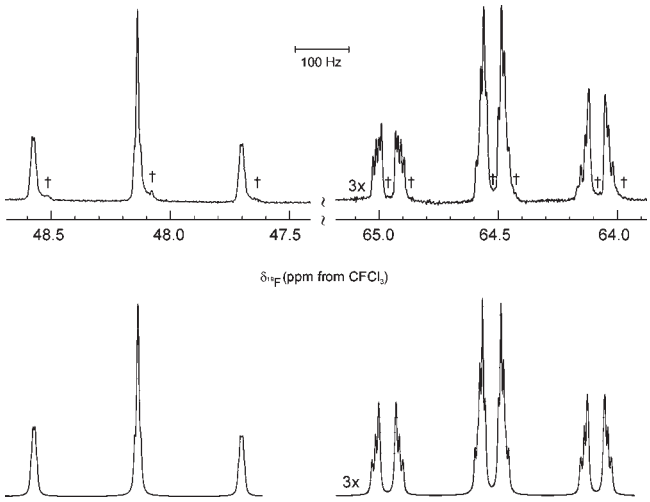

Figure 8. Experimental ^{19}F NMR spectrum (470.592 MHz) of $F_4S{=}NH_2^+$ in HF solvent at −20 °C (top traces) and simulated spectrum (bottom traces). The daggers (†) in the experimental spectrum denote the $^1\Delta^{19}F(^{34/32}S)$ secondary isotope shifts. Reproduced from ref 58.

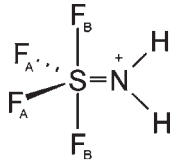

$A_2BB'XX'$

Structure II

$$[F_4S{=}NXe][AsF_6] + 2HF \xrightarrow[HF\ or\ BrF_5]{-20\ ^\circ C} [F_4S{=}NH_2][AsF_6] + XeF_2 \quad (3)$$

The ^{19}F NMR spectrum of $F_4S{=}NH_2^+$ (Figure 8) consists of an $A_2BB'XX'$ spin-coupling pattern (Structure II) with ^{19}F NMR parameters that are in a range similar to those of isoelectronic $F_4S{=}CH_2$,[63] but have chemical shifts that exhibit the opposite trend (NMR parameters for neat $F_4S{=}CH_2$ at −150 °C appear in square brackets in the ensuing discussion). Chemical shifts at 48.1 [59.0] (A_2) and 64.5 [53.6] (BB′) ppm arise from the $F_4S{=}N{-}$ group (local C_{2v} symmetry), with the additional fine structure on F_B arising from the protons (XX′) bonded to nitrogen. As previously noted for $F_4S{=}CH_2$,[63] two coupling paths between the F_B and H nuclei result from the high barrier to rotation about the S=N (S=C) double bond. Unfortunately, the ^{1}H NMR spectrum of $F_4S{=}NH_2^+$ was almost entirely obscured by overlap with the broad HF doublet [HF/BrF_5 solvent; −70 °C; $\delta(^1H)$ = 7.44 ppm; $^1J(^1H{-}^{19}F)$ = 470 Hz; $\Delta\nu_{1/2}$ = 700 Hz]. The ^{19}F spectral features arising from two $^{19}F{-}^1H$ coupling pathways were apparent in the ^{19}F NMR spectrum and were confirmed by spectral simulation (Figure 8). The F_A and F_B multiplets in the ^{19}F NMR spectrum consist of triplets that arise from $^2J(^{19}F_A{-}^{19}F_B)$ = 205.5 [154.4] Hz, with the F_A resonance being further split by $^3J(^{19}F_A{-}^1H)$ = −3.6 [10.5] Hz and the F_B resonance being further split by coupling through syn and anti hydrogen pathways, i.e., $^3J(^{19}F_B{-}^1H)_{syn}$ = 42.5 [58.1] Hz and $^3J(^{19}F_B{-}^1H)_{anti}$ = −1.1 [9.7] Hz. The appearances of these multiplets are also influenced by $^2J(^1H{-}^1H)$ (14.9 Hz). In contrast, the low-temperature spectrum of $(CH_3)_2NSF_4^+$

dx.doi.org/10.1021/ic201161q |Inorg. Chem. 2011, 50, 12359–12373

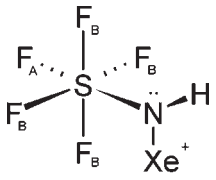

AB_4

Structure III

(−40 °C in SO_2) showed no evidence of hindered rotation about the S−N bond.[64]

(c) $F_5SN(H)Xe^+$. The salt $[F_5SN(H)Xe][AsF_6]$ was synthesized by solvolysis of $F_3S{\equiv}NXeF^+$ in aHF over a period of ca. 4 h at −20 °C (eq 4).[65] The salt was isolated as transparent yellow plates and was characterized by Raman spectroscopy at −45 °C. The $F_5SN(H)Xe^+$ cation was also formed by the reaction of $[F_5SNH_3][AsF_6]$ with XeF_2 in BrF_5 solvent (eq 5) at −30 °C for ca. 30 min and was characterized in solution by

$$[F_3S{\equiv}NXeF][AsF_6] + HF \xrightarrow[HF]{-20\ ^\circ C} [F_5SN(H)Xe][AsF_6] \quad (4)$$

$$[F_5SNH_3][AsF_5] + XeF_2 \underset{BrF_3}{\overset{30^\circ C}{\rightleftharpoons}} [F_5SN(H)Xe][AsF_6] + 2HF \quad (5)$$

^{19}F and ^1H NMR spectroscopy. In both cases, $F_5SNH_3^+$ and $F_5SN(H)Xe^+$ were observed in equilibrium with XeF_2 and HF (eq 5). In BrF_5 and aHF solutions below −20 °C, this equilibrium lies almost completely to the right, while in aHF above −20 °C, the reverse reaction is favored.

The ^{19}F NMR spectrum of the $F_5SN(H)Xe^+$ cation (Figure S1 in the Supporting Information) is an AB_4 spin-coupling pattern (Structure III), with the doublet at 71.3 (73.0) [F_A] ppm and the quintet at 59.0 (59.6) [F_B] ppm and $^2J(^{19}F_A-^{19}F_B)$ = 152.9 (154.7) Hz. These parameters are very similar to those of $F_5SNH_3^+$ (vide infra), except for the equatorial fluorine chemical shift, which is significantly more deshielded in the xenon cation, a trend that was also observed for the tellurium analogues $F_5TeN(H)Xe^+$ and $F_5TeNH_3^+$.[37]

The ^{129}Xe NMR spectrum of $F_5SN(H)Xe^+$ is a singlet [$\Delta\nu_{1/2}$ = 128 (150) Hz] at −2897 (−2956) ppm. The high ^{129}Xe shielding places the Xe−N bond among the most covalent Xe−N bonds known,[37,66] but this xenon environment is considerably less shielded than xenon in $C_6F_5Xe^+$ (−3831.5 ppm, HF solvent, −40 °C).[67] The ^{129}Xe shielding is very similar to that of its tellurium analogue (−2841 ppm, HF solvent, −45 °C; −2902 ppm, BrF_5 solvent, −48 °C) and $F_4S{=}NXe^+$ (−2674 ppm, vide infra). The resonances of these species are considerably more shielded than the ^{129}Xe resonances of $(FO_2S)_2NXeF$ (−1997 ppm, BrF_5 solvent, −58 °C),[40] $(SO_2F)_2NXe^+$ (−1943 ppm, SbF_5 solvent, 25 °C),[42] $F_3S{\equiv}NXeF^+$ (−1652 ppm, HF solvent, −20 °C; −1661 ppm, BrF_5 solvent, −60 °C),[45] isovalent F_5TeOXe^+ (−1472 ppm, SbF_5 solvent, 5 °C),[68] and XeF^+ (−574 ppm, SbF_5 solvent, 25 °C).[69] It has been shown that the ^{129}Xe shielding may be correlated with the L-group electronegativity and Xe−E bond covalency, where L is an electronegative ligand and E is a second-row ligand atom.[37,65] Accordingly, shielding generally increases with increasing Xe−E bond covalency for the series of LXe^+ cations, i.e., Xe−F < Xe−O < Xe−N < Xe−C. The $^{129}Xe-^{14}N$ coupling is not observed in $F_5SN(H)Xe^+$ because of quadrupolar relaxation of ^{14}N resulting from the low symmetry (high electric field gradient) at the nitrogen nucleus. The broad ^{129}Xe line widths of $F_5SN(H)Xe^+$ recorded at 11.7440 T precluded observation of the long-range couplings to xenon, namely, $^2J(^{129}Xe-^1H)$, $^3J(^{129}Xe-^{19}F_{ax})$, and $^3J(^{129}Xe-^{19}F_{eq})$, which also were not observed for $F_5TeN(H)Xe^+$.[37] The ^{129}Xe line width is largely attributable to relaxation of ^{129}Xe by shielding anisotropy (SA).

Because of ^1H chemical exchange and/or solvent overlap with the ^1H resonance of $F_5SN(H)Xe^+$, the spectrum was also recorded in BrF_5. The spectrum consisted of a singlet (9.57 ppm, −20 °C), but coupling to ^{14}N was not observed as a result of quadrupolar relaxation. Failure to observe the $^2J(^{129}Xe-^1H)$ coupling is also attributed to broadening of the ^{129}Xe satellites by a significant SA contribution to T_1 at the high external field strength used to obtain the ^1H NMR spectra.

(d) $F_5SNH_3^+$. In addition to solvolysis of $F_5SN(H)Xe^+$ (eq 5), $F_5SNH_3^+$ was also formed by HF addition to the S−N double bond of $F_4S{=}NH_2^+$ (eq 6)[58] and in a separate experiment by solvolysis of $F_3S{\equiv}NAsF_5$[17] in aHF at 0 °C for ca. 6 h (eq 7) as previously described.[25] The products were characterized by Raman spectroscopy at −160 °C and by ^{19}F and ^1H NMR spectroscopy.

$$[F_4S{=}NH_2][AsF_6] + HF \xrightarrow[HF]{-0\ ^\circ C} [F_5SNH_3][AsF_6] \quad (6)$$

$$[F_3S{\equiv}NAsF_5 + 3HF \xrightarrow[HF]{-0\ ^\circ C} [F_5SNH_3][AsF_6] \quad (7)$$

The ^{19}F NMR spectrum of $F_5SNH_3^+$ is an AX_4 spin system, occurring at 71.7 (73.8) [F_A] ppm and 50.1 (50.0) [F_X] ppm and $^2J(^{19}F_{ax}-^{19}F_{eq})$ = 152.6 (154.7) Hz. These parameters are in good agreement with those previously reported in SO_2; 76.37 and 52.43 ppm and 156.5 Hz (−40 °C), respectively.[25] The ^1H NMR spectrum is a broad singlet at 8.92 (7.74) ppm [$\Delta\nu_{1/2}$ = 23.0 (54.2) Hz], which is in agreement with that reported in SO_2; 8.8 ppm (−40 °C).[25] The line broadening and absence of resolved couplings is attributable to quadrupolar relaxation by the directly bonded ^{14}N atom (I = 1).

The $F_5SNH_3^+$ cation in aHF at 0 °C has been shown by ^{19}F NMR spectroscopy to undergo a further HF displacement reaction (eq 8), yielding SF_6 [$\delta(^{19}F)$ = 54.1 (56.0) ppm, $^1J(^{19}F-^{33}S)$ = 251.9 Hz] and the NH_4^+ cation [$\delta(^1H)$ = 5.54 ppm, $^1J(^1H-^{14}N)$ = 51 Hz].

$$[F_5SNH_3][AsF_6] + HF \xrightarrow[HF]{-20\ to\ 0\ ^\circ C} SF_6 + [NH_4][AsF_6] \quad (8)$$

(e) Solvolytic Pathways and Thermodynamic Considerations. Reaction pathways that account for the complex mixtures of cationic products and SF_6 observed in the ^{19}F NMR spectra of HF solutions of $F_3S{\equiv}NXeF^+$, along with their relative energies, are summarized in Scheme 2. Solvolysis of the $F_3S{\equiv}NXeF^+$ cation is likely initiated by HF-catalyzed rearrangement to $F_4S{=}NXe^+$ (Scheme 1), which was shown to occur at a much lower temperature (−20 °C) in aHF or aHF/BrF_5 solution than the solid-state rearrangement (22 °C; see Solid State Rearrangement of $[F_3S{\equiv}NXeF][AsF_6]$). Moreover, $F_3S{\equiv}NXeF^+$ does not undergo rearrangement in BrF_5 solvent at −20 °C in the absence of HF.[58]

Two pathways for HF solvolysis of $F_4S{=}NXe^+$ are possible: (1) the reaction with 2 equiv of HF to form $F_4S{=}NH_2^+$ and XeF_2 (eq 3) and (2) the addition of HF across the S=N double bond

dx.doi.org/10.1021/ic201161q |Inorg. Chem. 2011, 50, 12359–12373

Scheme 2. Calculated Relative Gas-Phase Energies of Products Resulting from the HF-Catalyzed Rearrangement of $F_3S{\equiv}NXeF^+$ and HF Solvolysis of $F_4S{=}NXe^+$ [kJ mol^{-1}; MP2/aug-cc-pVTZ(-PP)] (Adapted from Reference 58)

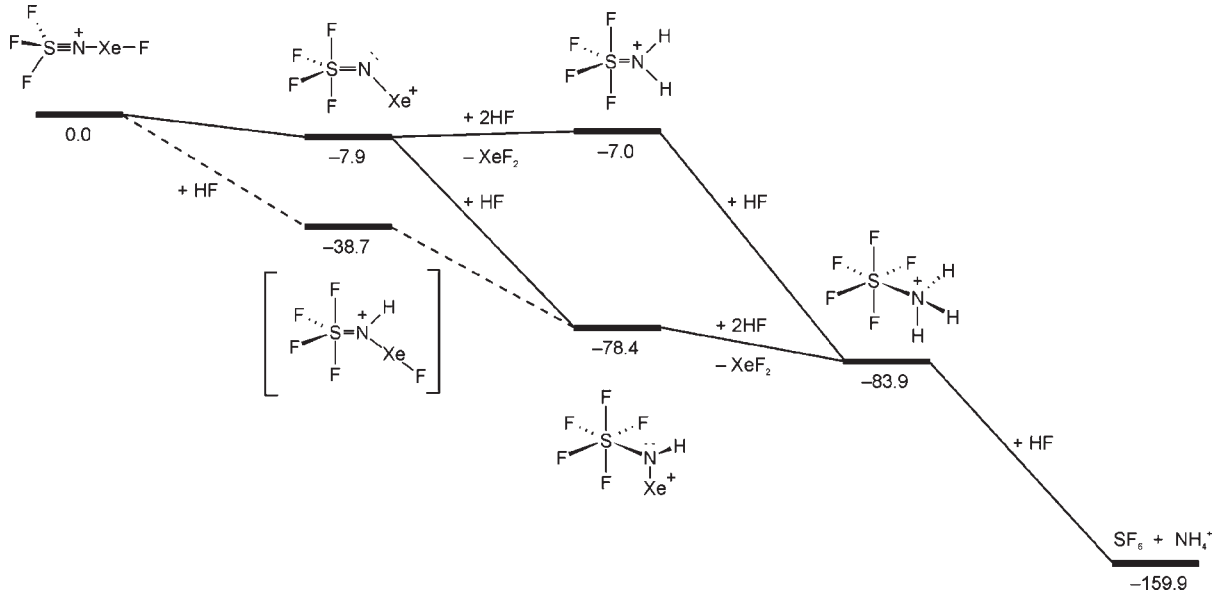

of $F_4S{=}NXe^+$ to give $F_5SN(H)Xe^+$ (eq 4). Each of these products may undergo further solvolysis by (1) the reaction of $F_5SN(H)Xe^+$ with 2 equiv of HF to form the very stable $F_5SNH_3^+$ cation and XeF_2 according to equilibrium (5) or (2) the addition of HF across the S=N double bond of $F_4S{=}NH_2^+$ to form $F_5SNH_3^+$ (eq 7). Fluorine-19 NMR spectroscopy shows that $F_5SN(H)Xe^+$ is initially formed, along with $F_4S{=}NXe^+$ and $F_4S{=}NH_2^+$, at −20 °C. The $F_5SN(H)Xe^+$ cation may result from HF addition across the $F_3S{\equiv}NXeF^+$ triple bond to form $F_4S{=}N(H)XeF^+$ as an intermediate, which rearranges to the more stable $F_5SN(H)Xe^+$ cation (Scheme 2). Although the $F_4S{=}N(H)XeF^+$ cation is thermodynamically favorable, presently there is no direct experimental evidence for its intermediacy. When the reaction mixture was warmed to 0 °C, $F_5SNH_3^+$ formation was favored while $F_4S{=}NXe^+$ was consumed and $F_4S{=}NH_2^+$ remained. Above 0 °C, $F_4S{=}NH_2^+$ was consumed and the $F_5SNH_3^+$ cation dominated (eqs 5 and 6), along with increasing amounts of its solvolysis products, SF_6 and NH_4^+ (eq 8), and a trace amount of F_5SNF_2, which was presumably generated by a series of reactions that are analogous to those described for the formation of F_5TeNF_2 during the decomposition of $F_5TeN(H)Xe^+$.[37]

(f) NMR Characterization of F_5SNH_2. Although F_5SNH_2 has been known for 45 years,[22] its NMR spectroscopic characterization is absent from the chemical literature. In the course of this work, the NMR parameters for F_5SNH_2 have been determined in $CH_3C{\equiv}N$ solvent at −20 °C: $\delta(^{19}F_{eq})$ = 72.9 ppm (doublet), $\delta(^{19}F_{ax})$ = 65.4 ppm (quintet), $^2J(^{19}F_{ax}{-}^{19}F_{eq})$ = 156.1 Hz, and $\delta(^1H)$ = 9.71 ppm (singlet).[16] The ^{19}F chemical shifts are deshielded with respect to those of $F_5SNH_3^+$ (72.1 and 58.9 ppm, respectively).[16]

III. Solid-State Structures of Cations Derived from $[F_3S{\equiv}NXeF][AsF_6]$. Although not explicitly discussed in this Article, the low-temperature Raman spectra of the title compounds have been obtained and fully assigned using frequencies and mode descriptions derived from quantum-chemical calculations. Also not explicitly discussed are the calculated gas-phase geometries of the cations and their ion pairs and correlations among geometric parameters and calculated charges, valencies, and bond orders derived from NBO analyses. References 45, 56, 58, and 65 should be consulted for detailed discussions of these studies. Key experimental bond lengths and bond angles are provided in the figure captions.

(a) Solid-State Rearrangement of $[F_3S{\equiv}NXeF][AsF_6]$. In addition to HF-catalyzed solution rearrangement, $[F_3S{\equiv}NXeF][AsF_6]$ undergoes solid-state rearrangement to $[F_4S{=}NXe][AsF_6]$. Rearrangement occurs upon warming of colorless, microcrystalline $[F_3S{\equiv}NXeF][AsF_6]$ to 22 °C (eq 9) and was monitored by

$$[F_3S{\equiv}NXeF][AsF_6] \xrightarrow{22\ ^\circ C} [F_4S{=}NXe][AsF_6] \qquad (9)$$

periodically quenching solid samples at −160 °C and recording their Raman spectra at this temperature. Monitoring of the most intense peaks in the Raman spectra [$F_3S{\equiv}NXeF^+$, ν(XeF), 550 cm^{-1}; $F_4S{=}NXe^+$, δ(XeNS), 178 cm^{-1}] showed that $F_4S{=}NXe^+$ formed as $F_3S{\equiv}NXeF^+$ was consumed but that the reaction was incomplete with no further reaction after ca. 70 min. The resulting bright-yellow solid was also characterized by ^{19}F NMR spectroscopy at −20 °C in $N{\equiv}SF_3$ solvent.[58]

A rationale for the rearrangement and for incomplete conversion of $F_3S{\equiv}NXeF^+$ to $F_4S{=}NXe^+$ is based on the crystal packing of $[F_3S{\equiv}NXeF][AsF_6]$, which shows a short cation-anion contact between a fluorine atom of the AsF_6^- anion and the sulfur atom of the $F_3S{\equiv}NXeF^+$ cation. This short contact is 2.871(5) Å,[45] compared to the sum of the fluorine and sulfur van der Waals radii (3.27 Å).[57] In the proposed reaction mechanism (Scheme 3), the sulfur atom of $F_3S{\equiv}NXeF^+$ undergoes nucleophilic attack by the AsF_6^- ion, which leads to fluoride ion transfer and the formation of the $[F_4S{=}NXe][AsF_6]$ ion pair. As the reaction proceeds, dilution of $F_3S{\equiv}NXeF^+$ and breakdown of the crystal lattice presumably disrupt fluoride ion transfer and rearrangement. The proposed rearrangement pathway is also consistent with the optimized,

dx.doi.org/10.1021/ic201161q |*Inorg. Chem.* 2011, 50, 12359–12373

Scheme 3. Proposed Solid-State Rearrangement of $[F_3S{\equiv}NXeF][AsF_6]$ Leading to $[F_4S{=}NXe][AsF_6]$ (Reproduced from Reference 58)

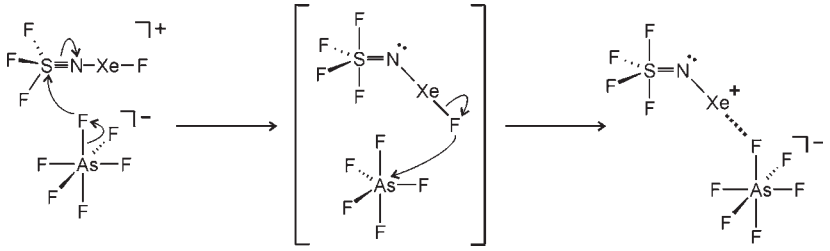

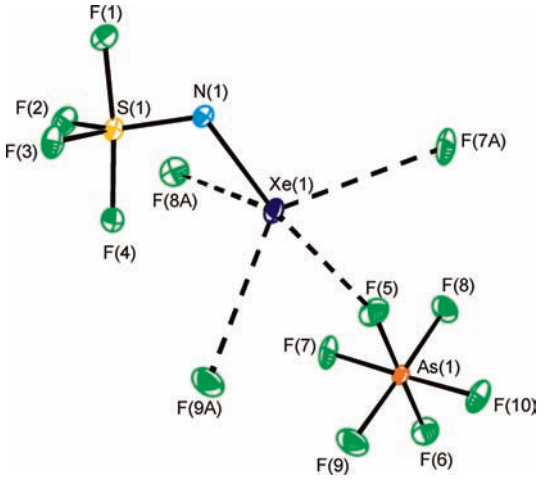

Figure 9. Structural unit in the X-ray crystal structure of $[F_4S{=}NXe][AsF_6]$ showing the closest contacts to xenon. Thermal ellipsoids are shown at the 50% probability level. Bond lengths (Å): S(1)−N(1), 1.556(3); S(1)−F(1), 1.576(2); S(1)−F(2), 1.518(2); S(1)−F(3), 1.529(2); S(1)−F(4), 1.588(2); Xe(1)−N(1), 2.084(3). Bond angles (deg): Xe(1)−N(1)−S(1), 118.0(2); N(1)−S(1)−F(1), 86.4(2); N(1)−S(1)−F(2), 127.3(2); N(1)−S(1)−F(3), 127.8(2); N(1)−S(1)−F(4), 100.1(2); N(1)−Xe(1)---F(5), 172.2(1). Contacts (Å): Xe(1)---F(5) 2.618(2); Xe(1)---F(7A), 3.226(3); Xe(1)---F(9A), 3.226(3); Xe(1)---F(8A), 3.232(3); Xe(1)---F(10A), 3.410(3); Xe(1)---F(7B), 3.452(3); Xe(1)---F(5A), 3.459(3). Reproduced from ref 58.

zero-point-corrected energies of the $F_3S{\equiv}NXeF^+$ and $F_4S{=}NXe^+$ cations, which show that $F_4S{=}NXe^+$ is 7.9 kJ mol^{-1} lower in energy than $F_3S{\equiv}NXeF^+$ at the MP2/aug-cc-pVTZ-(-PP) level of theory.[58]

(b) X-ray Crystal Structures of Cations that Contain the $F_4S{=}N-$ Group. The geometry of the $F_4S{=}N-$ group is derived from a trigonal-bipyramidal valence-shell electron-pair repulsion (VSEPR) arrangement of bonding pairs about sulfur, with the nitrogen and two fluorine atoms in the trigonal equatorial plane and two fluorine atoms in axial positions.

(i) $[F_4S{=}NXe][AsF_6]$. The $F_4S{=}NXe^+$ cation and the AsF_6^- anion form an ion pair by interaction through a Xe---F−As fluorine bridge (Figure 9).[58] The symmetry lowering experienced by the anion is shown in the crystal structure to be essentially an axial distortion of its O_h symmetry, giving an approximate local C_{4v} symmetry.

The Xe−N bond length is similar to that of $[F_5SN(H)Xe][AsF_6]$ [2.069(4) Å][65] and is only slightly longer than the Xe−N bond in $[F_5TeN(H)Xe][AsF_6]$ [2.044(4) Å; vide infra].[37] The xenon atom lies in the N(1)−S(1)−F(1)−F(4) plane, and the nonlinear S−N−Xe angle is attributed to the stereochemically active valence electron lone pair on nitrogen. The S−N bond length is significantly longer than those of $F_4S{=}NF$ [1.520(9) Å][60] and $F_4S{=}NCH_3$ [1.480(6) Å].[70] The axial S(1)−F(1) bond anti to xenon is longer than those in $F_4S{=}NCH_3$ [1.546(7) Å][70] and $F_4S{=}NF$ [1.535(12) Å],[60] while the syn-axial S(1)−F(4) bond length is shorter than the corresponding bonds in $F_4S{=}NCH_3$ [1.643(4) Å][70] and $F_4S{=}NF$ [1.615(7) Å].[60] The equatorial S(1)−F(2) and S(1)−F(3) bond lengths are also significantly shorter than those of $F_4S{=}NCH_3$ [1.567(4) Å][70] and $F_4S{=}NF$ [1.564(5) Å].[60]

The long contacts to xenon in the crystal structure may be grouped into three categories that are significantly less than the sum of the Xe and F van der Waals radii (3.63 Å):[57] (1) the short ion-pair contact, Xe(1)---F(5), which is trans to the Xe−N bond and similar to the corresponding contacts in $[F_5SN(H)Xe][AsF_6]$ [2.634(3) Å][65] and $[F_5TeN(H)Xe][AsF_6]$ [2.580(3) Å];[37] (2) three very similar contacts between xenon and three fluorine atoms of one anion [F(7A), F(9A), and F(8A)]; (3) three longer interionic contacts between xenon and fluorine atoms of two anions [F(10A), F(7B), and F(5A)]. The three contacts at 3.23 Å, when considered with the Xe−N bond and Xe---F ion pair contact, form a distorted trigonal-bipyramidal arrangement about xenon. The three equatorial fluorine contacts are not coplanar with xenon, which is displaced 1.226(2) Å out of the F(7A)−F(8A)−F(9A) plane toward the nitrogen atom, thus avoiding the torus of xenon valence electron density that results from its three valence electron lone pairs.[71]

(ii) $[F_4S{=}NH_2][AsF_6]$. The cations and anions of $[F_4S{=}NH_2][AsF_6]$ are well-separated in the crystal lattice (Figure 10), with two crystallographically independent anions that show little distortion from O_h symmetry.[58]

Although the electron densities of the sulfur ligand atoms are similar and the three equatorial bond lengths are similar, the nitrogen atom can be differentiated from the equatorial fluorine atoms based on the three equatorial bond angles; i.e., two F−S−N angles are equal within experimental error, with the third, smaller angle corresponding to the F−S−F angle. The crystallographic positions of the hydrogen atoms are calculated positions.

The S(1)−N(1) bond length of $F_4S{=}NH_2^+$ is bracketed by those of $F_4S{=}NCH_3$ [1.480(6) Å][70] and $F_4S{=}NF$ [1.520(9) Å][60] and is significantly shorter than those of $[F_4S{=}NXe][AsF_6]$ [1.556(3) Å][58] and $F_3SN(CH_3)_2$ [1.639(13) Å].[72] The axial S(1)−F(1) and S(1)−F(4) bond lengths of $F_4S{=}NH_2^+$ are the same within experimental error and are significantly shorter than those in $F_4S{=}NXe^+$ (vide supra) and in isoelectronic $F_4S{=}CH_2$

dx.doi.org/10.1021/ic201161q |*Inorg. Chem.* 2011, 50, 12359–12373

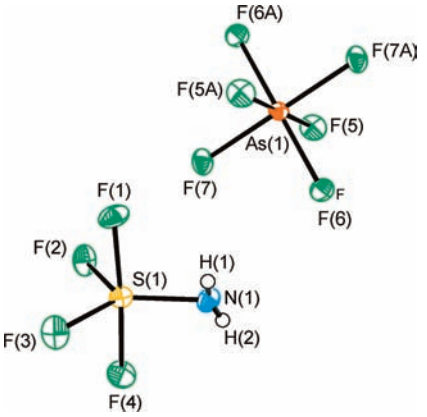

Figure 10. Structural unit in the X-ray crystal structure of $[F_4S{=}NH_2][AsF_6]$. The hydrogen atom positions are calculated, and the thermal ellipsoids of the non-hydrogen atoms are shown at the 50% probability level. Bond lengths (Å): S(1)−N(1), 1.511(6); S(1)−F(1), 1.564(5); S(1)−F(2), 1.511(5); S(1)−F(3), 1.526(5); S(1)−F(4), 1.558(5). Bond angles (deg): N(1)−S(1)−F(1), 92.6(3); N(1)−S(1)−F(2), 125.2(3); N(1)−S(1)−F(3), 126.3(3); N(1)−S(1)−F(4), 91.9(3). Contacts (Å): N(1)---F(10A), 2.824(3); N(1)---F(6), 2.841(3); N(1)---F(8), 2.916(3); N(1)---F(5A), 2.925(3). Reproduced from ref 58.

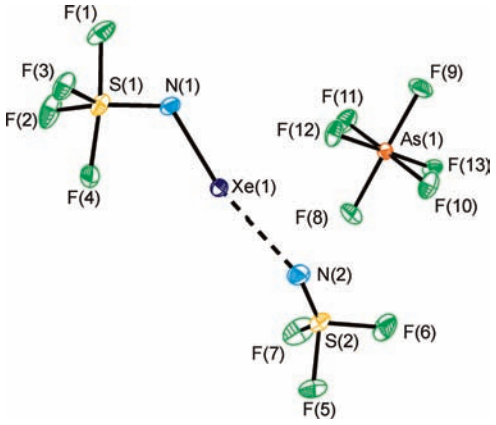

Figure 11. Structural unit in the X-ray crystal structure of $[F_4S{=}N{-}Xe{---}N{\equiv}SF_3][AsF_6]$. Thermal ellipsoids are shown at the 50% probability level. Bond lengths (Å): S(1)−N(1), 1.539(3); S(1)−F(1), 1.586(3); S(1)−F(2), 1.520(3); S(1)−F(3), 1.529(3); S(1)−F(4), 1.577(3); Xe(1)−N(1), 2.079(3); S(2)−N(2), 1.398(3); S(2)−F(5), 1.524(3); S(2)−F(6), 1.521(3); S(2)−F(7), 1.526(3). Bond angles (deg): Xe(1)−N(1)−S(1), 118.0(2); N(1)−S(1)−F(1), 87.6(2); N(1)−S(1)−F(2), 126.4(2); N(1)−S(1)−F(3), 128.2(2); N(1)−S(1)−F(4), 99.7(1), Xe(1)---N−S(2), 148.0(2), N(1)−Xe(1)---N(2), 168.4(1). Contacts (Å): Xe(1)---N(2), 2.583(3), F(3)---F(12), 2.755(4); F(3)---F(14), 2.757(4). Reproduced from ref 56.

[1.595(2) and 1.592(2) Å][73] and $F_4S{=}O$ [1.596(4) Å].[74] Similarly, the equatorial S(1)−F(2) and S(1)−F(3) bond lengths are comparable to those of $F_4S{=}NXe^+$ (vide supra) and $F_4S{=}O$ [1.533(4) Å],[74] while they are significantly shorter than those of $F_4S{=}CH_2$ [1.560(2) and 1.561(2) Å].[73]

(iii) $[F_4S{=}NXe{---}NSF_3][AsF_6]$. When [XeF][$AsF_6$] is allowed to react with a large excess of liquid $N{\equiv}SF_3$ by warming the mixture from −20 to 0 °C over ca. 15 h, the colorless $[F_3S{\equiv}NXeF][AsF_6]$ adduct salt that initially forms dissolves to give a deep-yellow solution that coincides with the formation of $[F_4S{=}N{-}Xe{---}N{\equiv}SF_3][AsF_6]$ (eq 10). Removal of excess $N{\equiv}SF_3$ under dynamic vacuum at −50 °C yielded an intense yellow solid, which was characterized by Raman spectroscopy at −160 °C.[56]

$$[F_3S{\equiv}NXeF][AsF_6] + N{\equiv}SF_3 \xrightarrow[N{\equiv}SF_3]{0\ ^\circ C} [F_4S{=}N{-}Xe{---}N{\equiv}SF_3][AsF_6] \quad (10)$$

The crystal structure of $[F_4S{=}N{-}Xe{---}N{\equiv}SF_3][AsF_6]$ consists of well-separated $F_4S{=}N{-}Xe{---}N{\equiv}SF_3^+$ cations and AsF_6^- anions (Figure 11), with the closest cation−anion contacts occurring between the equatorial fluorine F(3) of the cation and F(12) and F(14) of the anion, which are somewhat less than the sum of the fluorine van der Waals radii (2.94 Å).[57] The AsF_6^- anion shows little distortion from O_h geometry. The ligand arrangement around the sulfur atom of the cation is a distorted trigonal bipyramid, with the nitrogen and two fluorine atoms occupying the equatorial plane and two axial fluorine atoms approximately perpendicular to that plane. The xenon atom is coplanar with the orthogonal plane defined by the nitrogen, sulfur, and axial fluorine atoms, and the Xe−N=S angle is bent as a result of the sterically active electron lone pair on nitrogen.

The Xe(1)−N(1) bond length is equal, within $\pm 3\sigma$, to those of $[F_4S{=}NXe][AsF_6]$[58] and $[F_5SN(H)Xe][AsF_6]$,[65] somewhat longer than the Xe−N bond of $[F_5TeN(H)Xe][AsF_6]$,[37] but considerably shorter than the Xe−N bonds of the nitrogen base adducts of XeF^+ (vide infra). The S(1)−N(1) bond length of $F_4S{=}N{-}Xe{---}N{\equiv}SF_3^+$ is also equal, within experimental error, to those of $[F_4S{=}NXe][AsF_6]$[58] and $F_4S{=}NF$ [1.520(9) Å][60] but is longer than those of $F_4S{=}NH_2^+$ [1.511(6) Å][58] and $F_4S{=}NCH_3$ [1.480(6) Å].[70] All SF_4 bond lengths in $F_4S{=}N{-}Xe{---}N{\equiv}SF_3^+$ are the same, within $\pm 3\sigma$, as those of $[F_4S{=}NXe][AsF_6]$.[58] The Xe(1)−N(1)−S(1) and N(1)−S(1)−F(1) angles of $F_4S{=}N{-}Xe{---}N{\equiv}SF_3^+$ are slightly greater than those of $[F_4S{=}NXe][AsF_6]$ [118.0(2) and 86.4(2)°].[58] All other angles that are in common with the two structures are equal within ±0.9°. Detailed comparisons of the geometric parameters of $F_4S{=}NXe^+$ with those of $F_4S{=}NH_2^+$, $F_4S{=}NCH_3$, and $F_4S{=}NF$ are provided in ref 58.

The short Xe(1)---N(2) contact is well within the sum of the nitrogen and xenon van der Waals radii (3.71 Å)[57] but considerably longer than the Xe−N bond lengths of the related cations $[F_3S{\equiv}NXeF][AsF_6]$ [2.236(4) Å],[45] $[HC{\equiv}NXeF][AsF_6]$ [2.235(3) Å],[47] $[(CH_3)_3C{\equiv}NXeF][AsF_6]$ [2.212(4) Å],[47] and $[CH_3C{\equiv}NXeF][AsF_6]{\cdot}HF$ [2.179(7) Å][47] while somewhat shorter than the Xe---N contacts in the $CH_3C{\equiv}N$ solvated salts of the more weakly acidic $C_6F_5Xe^+$ cation, $[C_6F_5Xe{---}N{\equiv}CCH_3][B(C_6F_5)_4]$ [2.610(11) Å],[75] $[C_6F_5Xe{---}N{\equiv}CCH_3][B(CF_3)_4]$ [2.640(6) Å],[75] $[C_6F_5Xe{---}N{\equiv}CCH_3][(C_6F_5)_2BF_2]$ [2.681(8) Å],[76] and $[C_6F_5Xe{---}NC_5H_3F_2][AsF_6]$ [2.694(5) Å].[77] The donor-acceptor bond length trends are in accordance with the gas-phase donor-acceptor dissociation energies calculated for $F_3S{\equiv}NXeF^+$, $HC{\equiv}NXeF^+$, $F_4S{=}N{-}Xe{---}N{\equiv}SF_3^+$, and $F_3S{\equiv}NAsF_5$.[56]

The deviation of the Xe(1)---N(2)−S(2) angle from linearity is similar to that observed for this angle in $[F_3S{\equiv}NXeF][AsF_6]$ [142.6(3)°][45] and is likewise attributable to crystal packing. The N(1)−Xe(1)---N(2) angle deviates less from linearity. The observed and calculated low frequencies of the Xe---N≡S and N−Xe---N bending modes show that these angles are highly deformable and that their nonlinearities likely arise from crystal packing.[56]

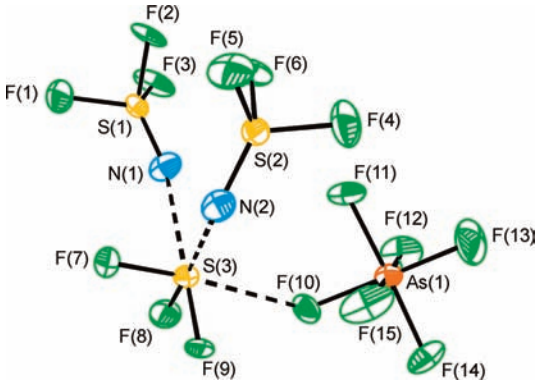

Figure 12. Structural unit in the X-ray crystal structure of $[F_3S(N{\equiv}SF_3)_2][AsF_6]$. Thermal ellipsoids are shown at the 50% probability level. Bond lengths (Å): S(3)−F(7), 1.511(1); S(3)−F(8), 1.519(1); S(3)−F(9), 1.520(1); S(1)−N(1), 1.539(3); S(1)−F(1), 1.518(2); S(1)−F(2), 1.521(1); S(1)−F(3), 1.518(2); S(2)−N(2), 1.392(2); S(2)−F(4), 1.516(2); S(2)−F(5), 1.525(2); S(2)−F(6), 1.525(2). Bond angles (deg): F(7)−S(3)−F(8), 96.2(1); F(7)−S(3)−F(9), 96.8(1); F(8)−S(3)−F(9), 96.3(1); N(1)---S(3)---N(2), 96.3(1); N(1)---S(3)---F(10), 97.7(1); N(2)---S(3)---F(10), 104.4(1). Contacts (Å): S(3)---N(1), 2.554(2), S(3)---N(2), 2.511(2); S(3)---F(10), 2.558(2). Reproduced from ref 56.

The S(2)−N(2) and average S−F bond lengths of adducted $N{\equiv}SF_3$ in $F_4S{=}N{-}Xe{---}N{\equiv}SF_3^+$ are shorter than those in gaseous $N{\equiv}SF_3$ [S−N, 1.416(3) Å; S−F, 1.552(6) Å].[14] Similar S≡N and S−F bond-length contractions have been observed in other main-group adducts, namely, $F_3S{\equiv}NAsF_5$ (1.383 and 1.439 Å)[5] and $[F_3S{\equiv}NXeF][AsF_6]$ [1.397(5) and 1.503(3) Å][45] and in the transition-metal adducts $[Mn(N{\equiv}SF_3)_4][AsF_6]_2$ [1.365(11) and 1.506(5) Å][53] and $[Re(CO)_5N{\equiv}SF_3][AsF_6]$ [1.384(14) and 1.499(10) Å].[54]

The N−S−F and F−S−F angles in the adducted $N{\equiv}SF_3$ molecule average 121.4(2) and 95.4(2)°, respectively, comprising a distorted tetrahedral arrangement about sulfur that is similar to those of $N{\equiv}SF_3$[14,15] and its adducts.[5,45,53,54]

(iv) $[F_3S(N{\equiv}SF_3)_2][AsF_6]$. When the growth of single crystals of $[F_4S{=}N{-}Xe{---}N{\equiv}SF_3][AsF_6]$ was attempted from $N{\equiv}SF_3$ solvent at 0 °C, colorless $[F_3S(N{\equiv}SF_3)_2][AsF_6]$ crystals were also obtained and were characterized by Raman spectroscopy and single-crystal X-ray diffraction. This salt resulted from redox decomposition of the $F_4S{=}NXe^+$ cation at 0 °C (eq 11) and liberated Xe and *cis*-N_2F_2.[56]

$$[F_4S{=}N{-}Xe{---}N{\equiv}SF_3][AsF_6] + N{\equiv}SF_3 \xrightarrow[N{\equiv}SF_3]{0\ ^\circ C} [F_3S(N{\equiv}SF_3)_2][AsF_6] + Xe + \tfrac{1}{2}cis\text{-}N_2F_2 \quad (11)$$

The crystal structure of $[F_3S(N{\equiv}SF_3)_2][AsF_6]$ consists of an SF_3^+ cation having three long contacts to S^{IV}: one from a fluorine atom of a neighboring AsF_6^- anion and two from the nitrogen atoms of the $N{\equiv}SF_3$ molecules (Figure 12). When the S---N and S---F contacts are ignored, the SF_3^+ cation has a symmetry very close to C_{3v}, as has been observed for $[SF_3][BF_4]$[78] and $[SF_3]_2[GeF_6]$,[79] the only other SF_3^+ salts to have been structurally characterized by single-crystal X-ray diffraction. In the latter salts, the S^{IV} coordination sphere includes three long contacts to fluorine ligands of their anions. As in the $[SF_3][BF_4]$ and $[SF_3]_2[GeF_6]$ salts, the long $S^{IV}{\cdots}F$ contacts avoid the fluorine atoms and the nonbonding electron pair situated on the 3-fold axis of SF_3^+, providing distorted octahedral coordination around the S^{IV} atom.

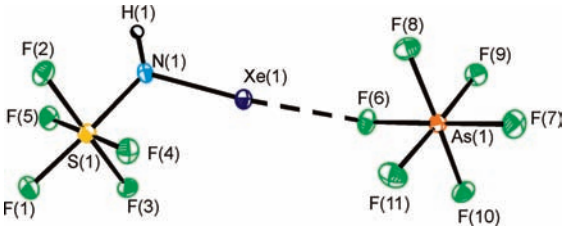

Figure 13. X-ray crystal structure of $[F_5SN(H)Xe][AsF_6]$. Thermal ellipsoids are shown at the 50% probability level. Bond lengths (Å): S(1)−N(1), 1.761(4); S(1)−F(1), 1.559(3); S(1)−F(2), 1.565(3); S(1)−F(3), 1.578(3); S(1)−F(4), 1.578(3); S(1)−F(5), 1.571(3); Xe(1)−N(1), 2.069(4). Bond angles (deg): Xe(1)−N(1)−S(1), 115.3(2); N(1)−S(1)−F(1), 176.7(2); N(1)−S(1)−F(2), 87.4(2); N(1)−S(1)−F(3), 94.0(2); N(1)−S(1)−F(4), 88.5(2), N(1)−S(1)−F(5), 90.7(2), N(1)−Xe(1)---F(6), 171.6(1). Contacts (Å): Xe(1)---F(6), 2.634(4), Xe(1)···F(6A), 3.342 Å, Xe(1)···F(6B), 3.387, Xe(1)···F(5A), 3.271, Xe(1)···F(2A), 3.267, Xe(1)···F(1A), 3.376, Xe(1)···F(1B), 3.225. Reproduced from ref 65.

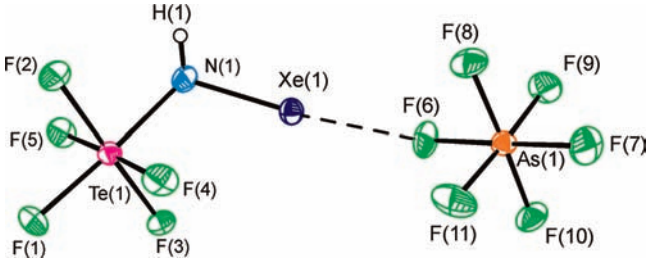

Figure 14. X-ray crystal structure of $[F_5TeN(H)Xe][AsF_6]$. Thermal ellipsoids are shown at the 50% probability level. Bond lengths (Å): Te(1)−N(1), 1.928(5); Te(1)−F(1), 1.791(4); Te(1)−F(2), 1.820(3); Te(1)−F(3), 1.819(3); Te(1)−F(4), 1.801(4); Te(1)−F(5), 1.805(4); Xe(1)−N(1), 2.044(4). Bond angles (deg): Xe(1)−N(1)−Te(1), 115.1(2); N(1)−Te(1)−F(1), 176.6(2); N(1)−Te(1)−F(2), 90.1(2); N(1)−Te(1)−F(3), 88.2(2); N(1)−Te(1)−F(4), 88.6(2); N(1)−Te(1)−F(5), 94.2(2). Contacts (Å): Xe(1)---F(6), 2.580(3); Xe(1)---F(5), 3.169; Xe(1)---F(6A), 3.281; Xe(1)---F(11B), 3.265; Xe(1)---F(10E), 3.260. Reproduced from ref 37.

The S(3)−F bond lengths in $[F_3S(N{\equiv}SF_3)_2][AsF_6]$ are equal, within experimental error, to those in $[SF_3]_2[GeF_6]$ [1.515(2), 1.519(2), and 1.519(2) Å][79] and to the thermally corrected values of $[SF_3][BF_4]$ [1.518, 1.518, and 1.514 Å].[78] The F−S−F bond angles of the SF_3^+ cation are in agreement with those of $[SF_3]_2[GeF_6]$[79] and $[SF_3][BF_4]$[78] and are significantly greater than 90°, as is predicted for the gas-phase cation (94.5, 94.5, and 95.0°). The short S(3)---F(10) contact between SF_3^+ and a fluorine of AsF_6^- is well within the sum of the sulfur and fluorine van der Waals radii (3.27 Å).[57] The short S---N contacts between SF_3^+ and the nitrogen atoms of the $N{\equiv}SF_3$ molecules are significantly less than the sum of the sulfur and nitrogen van der Waals radii (3.35 Å)[57] and are similar to the S---F contact distance. The N---S(3)---N [96.3(1)°] and F---S(3)---N [97.7(1) and 104.4°] angles are significantly greater than 90°, forming a distorted octahedral geometry about sulfur such that the contacts to $N{\equiv}SF_3$ and AsF_6^- avoid the stereochemically active valence electron lone pair and fluorine ligands of SF_3^+ to

dx.doi.org/10.1021/ic201161q |*Inorg. Chem.* 2011, 50, 12359–12373

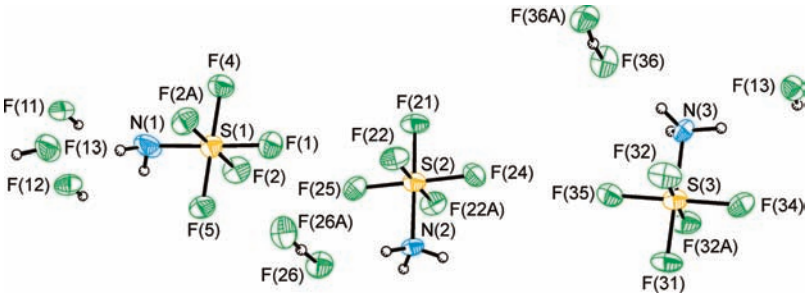

Figure 15. Structural unit in the X-ray crystal structure of $F_5SNH_2 \cdot 2[F_5SNH_3][HF_2] \cdot 4HF$. Thermal ellipsoids are shown at the 50% probability level. Bond lengths (Å): F_5SNH_2, S(1)−N(1), 1.716(8); S(1)−F(1), 1.552(5); S(1)−F(2), 1.568(4); S(1)−F(4), 1.579(5); S(1)−F(5), 1.560(5); $F_5SNH_3^+$, S(2)−N(2), 1.717(7); S(2)−F(21), 1.559(5); S(2)−F(22), 1.557(3); S(2)−F(24), 1.560(5); S(2)−F(25), 1.559(5); S(3)−N(3), 1.739(7); S(3)−F(31), 1.551(5); S(3)−F(32), 1.564(3); S(3)−F(34), 1.550(5); S(3)−F(35), 1.558(5). Bond angles (deg): F_5SNH_2, N(1)−S(1)−F(1), 178.4(3); N(1)−S(1)−F(2), 90.1(2); N(1)−S(1)−F(4), 89.2(3); N(1)−S(1)−F(5), 91.4(3); $F_5SNH_3^+$, N(2)−S(2)−F(21), 179.2(3); N(2)−S(2)−F(22), 90.3(1); N(2)−S(2)−F(24), 91.2(3); N(2)−S(2)−F(25), 89.4(3); N(3)−S(3)−F(31), 179.7(3); N(3)−S(3)−F(32), 89.8(1); N(3)−S(3)−F(34), 91.0(3); N(3)−S(3)−F(35), 89.1(3). Reproduced from ref 16.

the maximum extent. The bond lengths and angles of the adducted $N{\equiv}SF_3$ molecules again show the expected decreases[5] relative to those of $N{\equiv}SF_3$[14,15] and are very similar to those of adducted $N{\equiv}SF_3$ in $F_4S{=}N{-}Xe{---}N{\equiv}SF_3^+$ and in related adducts (vide supra).

(c) X-ray Crystal Structures of F_5SN- Derivatives. The geometry of the F_5SN- group is derived from an octahedral arrangement of bonding pairs about sulfur, with four fluorine atoms in the equatorial plane and the nitrogen and one fluorine atom in axial positions.

(i) $[F_5SN(H)Xe][AsF_6]$. The $F_5SN(H)Xe^+$ cation and AsF_6^- anion form an ion pair by interaction through a Xe--F−As fluorine bridge (Figure 13) in which the AsF_6^- anion is distorted from O_h to approximate local C_{4v} symmetry (see III(b)(i) $[F_4S{=}NXe][AsF_6]$ and III(b)(iii), $[F_4S{=}NXe{---}NSF_3][AsF_6]$).

In $[F_5SN(H)Xe][AsF_6]$, the Xe(1)−N(1) and Xe(1)---F(6) bond lengths are somewhat longer than their counterparts in $[F_5TeN(H)Xe][AsF_6]$ (Figure 14), while the Xe(1)−N(1)−H(1), N(1)−Xe(1)---F(6), and S/Te−N−Xe angles are equal within experimental error. As expected, the S−N, S−F_{ax}, and average S−F_{eq} bond lengths are shorter, by 0.23 ±0.01 Å, when compared with the analogous bond lengths in $[F_5TeN(H)Xe][AsF_6]$.

The fluorine contacts to xenon in $F_5SN(H)Xe^+$ are within the sum of fluorine and xenon van der Waals radii (3.63 Å)[57] and avoid the torus of electron density around Xe^{II}.[71] These contacts may also contribute to the distortion of the N−Xe---F angle from the expected linear AX_2E_3 VSEPR arrangement; however, a similar deviation from linearity was obtained in the energy-minimized gas-phase geometries, and for the F−Ng---F angles (Ng = Kr, Xe) in $Kr_2F_3^+$,[80] $Xe_2F_3^+$,[46] and $[KrF][MF_6]$ (M = As, Sb, Bi),[80] and therefore may not be wholly attributable to crystal packing. The Xe---F(6)−As bridge bond angle is comparable to that in $[F_5TeN(H)Xe][AsF_6]$[37] and is consistent with the bent geometry predicted by the VSEPR model and with the observed range of Ng---F−As (Ng = Xe, Kr) angles in $[XeF][AsF_6]$,[49] $HF \cdot [HO\text{-}TeF_4OXe][AsF_6]$,[81] $[KrF][AsF_6]$,[80] $[Kr_2F_3][AsF_6] \cdot [KrF][AsF_6]$,[80] and $[C_6F_5Xe][AsF_6]$.[82]

(ii) $F_5SNH_2 \cdot [F_5SNH_3][AsF_6] \cdot 4HF$. Pentafluorosulfanyamine, F_5SNH_2, prepared by a method similar to that previously described[22] (eq 12), forms colorless solutions in aHF. Slow removal of HF

$$N{\equiv}SF_3 + 2HF \xrightarrow[HF]{0\ ^\circ C} F_5SNH_2 \qquad (12)$$

under dynamic vacuum at −65 °C yields $F_5SNH_2 \cdot n$HF as a white powder, which is stable at −78 °C. Static sublimation under 1 atm of dry N_2 at −30 to −35 °C affords single crystals of $F_5SNH_2 \cdot 2[F_5SNH_3][HF_2] \cdot 4HF$ (Table S1 in the Supporting Information).[16] The formation of this compound is presumably driven by the lattice energy, which is dominated by salt formation and hydrogen bond formation (eq 13). No evidence for $[F_5SNH_3][HF_2]$ was observed for the powdered sample by Raman spectroscopy prior to sublimation.

$$3F_5SNH_2 + 8HF \xrightarrow{30\ ^\circ C} F_5SNH_2 \cdot 2[F_5SNH_3][HF_2] \cdot 4HF \qquad (13)$$

The crystal structure of $F_5SNH_2 \cdot 2[F_5SNH_3][HF_2] \cdot 4HF$ (Figure 15) consists of well-separated F_5SNH_2 molecules and two crystallographically independent $F_5SNH_3^+$ cations, which are linked by N−H---F hydrogen-bonding interactions through HF molecules and HF_2^- anions. The HF_2^- anions show little distortion from linearity, with F---H---F bond angles of 172.7 and 177.4° and F---F distances of 2.325(8) and 2.329(8) Å, in good agreement with previously reported values.[83−85]

The N−S and S−F bond lengths are equal, within ±3σ, in F_5SNH_2 and both $F_5SNH_3^+$ cations. The N−S bond lengths are shorter, but the S−F bond lengths are similar to those of $F_5SN(H)Xe^+$ in $[F_5SN(H)Xe][AsF_6]$ [1.761(4) and 1.559(3)−1.578(3) Å].[65]

Hydrogen-bonding interactions involving F_5SNH_2 and $F_5SNH_3^+$ only occur between the hydrogen atoms bonded to nitrogen and the fluorine atoms of HF or HF_2^- (the sum of the hydrogen and fluorine van der Waals radii is 2.67 Å).[57] The hydrogen atoms of F_5SNH_2 hydrogen bond to F(26) and F(36) of each HF_2^- anion (1.926 and 2.503 Å) and to F(10) of the ordered HF molecule (2.524 Å). The H(20) and H(30) atoms of the two $F_5SNH_3^+$ cations each interact with F(11) (1.916 and 2.595 Å) and F(13) (2.555 and 1.928 Å) of disordered HF molecules, while H(2) and H(2A) interact with F(26) (1.797 Å) and F(13) (2.574 Å) and H(3) and H(3A) interact with F(36) (1.781 Å) and F(11) (2.563 Å). The resulting hydrogen-bonded rings pack on top of each other to give channels that run along the *b*-axis in the extended crystal structure (Figure S2a in the Supporting Information). These channels are occupied by the more weakly interacting [F(10)] and noninteracting [F(12)] HF molecules. When viewed along the *c*-axis, these rings are joined by hydrogen

dx.doi.org/10.1021/ic201161q |*Inorg. Chem.* 2011, 50, 12359–12373

bonds between the HF_2^- anions and both F_5SNH_2 and $F_5SNH_3^+$, which form a network of smaller rings (Figure S2b in the Supporting Information).

CONCLUSION

Since the discovery of $N{\equiv}SF_3$ more than 50 years ago, numerous papers reporting the properties and chemistry of this fascinating molecule have appeared that span the donor and acceptor properties of its nitrogen and sulfur centers, respectively, the saturation of the S≡N triple bond, and the nucleophilic substitution of the fluorine ligands bonded to sulfur. Although it appeared that the chemistry of $N{\equiv}SF_3$ had been extensively studied, the research dealt with in this account has shown that synthetic approaches that mainly rely upon HF solvolyses have opened new avenues to Xe−N bond formation that have been of fundamental importance to the development of noble-gas chemistry. At first glance, the reaction of the Lewis acidic XeF^+ cation with $N{\equiv}SF_3$ seemed only to add a further example, $F_3S{\equiv}NXeF^+$, to the large number of nitrogen base XeF^+ adducts that were already known, but it was shown that a further and extensive chemistry is possible with the coordinated $N{\equiv}SF_3$ ligand. In aHF, $F_3S{\equiv}NXeF^+$ undergoes rearrangement to $F_4S{=}NXe^+$, from which two further reaction channels emerge: (1) the addition of HF across the S=N bond and (2) the addition of HF across the Xe−N bond. The addition of one or three HF molecules across the S=N bond has yielded $F_5SN(H)Xe^+$ and $F_5SNH_3^+$(together with XeF_2) respectively. The addition of a further two HF molecules across the Xe−N bond of $F_4S{=}NXe^+$ results in Xe−N bond cleavage to give the novel $F_4S{=}NH_2^+$ cation and XeF_2. These species have been characterized in situ by multi-NMR spectroscopy and in the solid state by Raman spectroscopy and single-crystal X-ray structure determinations, with the experimental results supported by quantum-chemical calculations. The relative Xe−N bond covalencies of $F_4S{=}NXe^+$, $F_5SN(H)Xe^+$, and $F_5TeN(H)Xe^+$ have been assessed on the basis of their Xe−N bond lengths and ^{129}Xe NMR shieldings and are among the most covalent Xe−N bonds presently known. Moreover, $[F_4S{=}NXe{\cdots}N{\equiv}SF_3][AsF_6]$, $[F_3S(N{\equiv}SF_3)_2][AsF_6]$, and $F_5SNH_2{\cdot}2[F_5SNH_3][AsF_6]{\cdot}4HF$ have been characterized. The complex salt $F_5SNH_2{\cdot}2[F_5SNH_3][AsF_6]{\cdot}4HF$ has added significant structural detail to the somewhat limited characterization of F_5SNH_2 and $F_5SNH_3^+$.

OUTLOOK

In addition to providing further examples of Xe^{II}−N bonds, $N{\equiv}SF_3$ may provide avenues to the syntheses of nitrogen-bonded derivatives of Xe^{IV} and Xe^{VI}. The only published example of Xe^{IV} bonded to nitrogen is the weakly coordinated $F_2OXe{\cdots}N{\equiv}CCH_3$ adduct,[86] whereas a Xe^{VI}−N-bonded derivative has not yet been reported. The syntheses of krypton analogues of the Xe^{II} derivatives described in this Article promise to be among the most challenging.

The F_5TeO- (teflate) group is known to have chemistry and electronegativity similar to those of fluorine.[87] The teflate analogue of XeF^+, $XeOTeF_5^+$, has a Lewis acidity comparable to that of XeF^+ and can reasonably be expected to form the $F_3S{\equiv}NXeOTeF_5^+$ cation in its reaction with $N{\equiv}SF_3$. A study of HF the solvolysis of the $F_3S{\equiv}NXeOTeF_5^+$ cation, by analogy with that of $F_3S{\equiv}NXeF^+$, is not possible because HF solvolysis would result in $HOTeF_5$ displacement. However, an analogous solid-state rearrangement (see Scheme 3) may occur, yielding $F_3(OTeF_5)S{=}NXe^+$, which could exist as a mixture of up to three isomers and should lead to a better understanding of the solid-state rearrangement mechanism of $F_3S{\equiv}NXeF^+$.

The interaction of a $F_5SN(H)Xe^+$ salt with liquid $N{\equiv}SF_3$ can be expected to form the donor-acceptor adduct $[F_5SN(H)Xe{\cdots}N{\equiv}SF_3][AsF_6]$ by analogy with $[F_4S{=}NXe{\cdots}N{\equiv}SF_3][AsF_6]$. This would provide only the third known compound containing a N−Xe−N linkage and a further example of xenon bound to an inorganic sp^3-hybridized nitrogen center.

Thiazyl trifluoride may be sufficiently resistant to oxidative attack by xenon in the +4 oxidation state. The low-temperature reaction of the known $[XeF_3][SbF_6]$ salt[88,89] with excess liquid $N{\equiv}SF_3$ may yield the $F_3S{\equiv}NXeF_3^+$ cation. Hydrogen fluoride solvolysis of $F_3S{\equiv}NXeF_3^+$ could lead to the $F_4S{=}NXeF_2^+$ and $F_5SN(H)XeF_2^+$ cations, significantly extending the known chemistry of Xe^{IV} by providing the first strongly covalent Xe^{IV}−N bonded species. Similar synthetic approaches may be applicable in the development of an analogous Xe^{VI} chemistry and the formation of the first Xe^{VI}−N bonds, namely, the $F_4S{=}NXeF_4^+$ and $F_5SN(H)XeF_4^+$ cations.

The chemistry of krypton is limited to the +2 oxidation state, but Kr^{II} chemistry is in many ways analogous to that of Xe^{II}; however, far fewer Kr^{II} compounds are known because they are endothermic and possess significantly stronger oxidizing properties.[49,90] Thiazyl trifluoride may prove to be sufficiently resistant to oxidative attack by Kr^{II} to allow the syntheses of kinetically stable $F_3S{\equiv}NKrF^+$, $F_4S{=}NKr^+$, and $F_5SN(H)Kr^+$ by low-temperature routes that are closely analogous to those used for the syntheses of the Xe^{II} analogues.

ASSOCIATED CONTENT

Supporting Information. Fluorine-19 NMR spectrum of $F_5SN(H)Xe^+$ in HF solvent, synthesis of $F_5SNH_2{\cdot}n$HF (Figure S1), crystal growth of $F_5SNH_2{\cdot}2[F_5SNH_3][AsF_6]{\cdot}4HF$, crystal packing diagrams for $F_5SNH_2{\cdot}2[F_5SNH_3][HF_2]{\cdot}4HF$ showing the hydrogen-bonding interactions (Figure S2), and a summary of crystal data and refinement results for $F_5SNH_2{\cdot}2[F_5SNH_3][HF_2]{\cdot}4HF$ (Table S1). This material is available free of charge via the Internet at http://pubs.acs.org.

AUTHOR INFORMATION

Corresponding Author

*E-mail: schrobil@mcmaster.ca.

ACKNOWLEDGMENT

This article is dedicated to our friend and colleague Professor Dr. Rüdiger Mews in recognition of his lifetime achievements and contributions to the chemistry of sulfur-nitrogen fluorides. We thank the Natural Sciences and Engineering Research Council of Canada for financial support in the form of a Discovery Grant (to G.J.S.) and the Ontario Ministry of Training, Colleges and Universities and McMaster University for the award of graduate scholarships (to G.L.S.).

REFERENCES

(1) Glemser, O.; Schröder, H.; Haeseler, H. *Z. Anorg. Allg. Chem.* **1955**, *279*, 28–37.

(2) Glemser, O.; Schröder, H. *Z. Anorg. Allg. Chem.* **1956**, *284*, 97–100.
(3) Glemser, O.; Mews, R. *Adv. Inorg. Chem. Radiochem.* **1972**, *14*, 333–390.
(4) Mews, R. *Adv. Inorg. Chem. Radiochem.* **1976**, *19*, 185–237.
(5) Glemser, O.; Mews, R. *Angew. Chem., Int. Ed. Engl.* **1980**, *19*, 883–899.
(6) Roesky, H. W. *J. Fluorine Chem.* **1999**, *100*, 217–226.
(7) Thrasher, J. S. *Inorg. Synth.* **1986**, *24*, 99–101.
(8) Thrasher, J. S. *Inorg. Synth.* **1986**, *24*, 10–12.
(9) Mews, R.; Keller, K.; Glemser, O. *Inorg. Synth.* **1986**, *24*, 12–17.
(10) Glemser, O.; Richert, H. *Z. Anorg. Allg. Chem.* **1961**, *307*, 313–327.
(11) Richert, H.; Glemser, O. *Z. Anorg. Allg. Chem.* **1961**, *307*, 328–344.
(12) Koeniger, F.; Müller, A.; Glemser, O. *J. Mol. Struct.* **1978**, *46*, 29–34.
(13) Müller, A.; Ruoff, A.; Krebs, B.; Glemser, O.; Koch, W. *Spectrochim. Acta, Part A* **1969**, *25*, 199–205.
(14) Kirchhoff, W. H.; Wilson, E. B., Jr. *J. Am. Chem. Soc.* **1962**, *84*, 334–336.
(15) Borrmann, T.; Lork, E.; Mews, R.; Parsons, S.; Petersen, J.; Stohrer, W.-D.; Watson, P. G. *Inorg. Chim. Acta* **2008**, *361*, 479–486.
(16) Smith, G. L. Ph.D. Thesis, McMaster University, Hamilton, Ontario, Canada, 2010.
(17) Glemser, O.; Koch, W. *An. Asoc. Quim. Argent.* **1971**, *59*, 143–148.
(18) Müller, A.; Glemser, O.; Scherf, K. *Chem. Ber.* **1966**, *99*, 3568–3571.
(19) Erhart, M.; Mews, R. *Z. Anorg. Allg. Chem.* **1992**, *615*, 117–122.
(20) Mews, R. *J. Chem. Soc., Chem. Commun.* **1979**, 278–279.
(21) Braeuer, H. C. *Diplomarbeit*; Universität Göttingen, Göttingen, Germany, 1977.
(22) Clifford, A. F.; Duncan, L. C. *Inorg. Chem.* **1966**, *5*, 692–693.
(23) Clifford, A. F.; Zeilenga, G. R. *Inorg. Chem.* **1969**, *8*, 979–980.
(24) Bartsch, R.; Henle, H.; Meier, T.; Mews, R. *Chem. Ber.* **1988**, *121*, 451–456.
(25) Meier, T.; Hoppenheit, R.; Mews, R. *Z. Anorg. Allg. Chem.* **1993**, *619*, 1241–1246.
(26) Roesky, H. W.; Glemser, O.; Hoff, A.; Koch, W. *Inorg. Nucl. Chem. Lett.* **1967**, *3*, 39–42.
(27) Mews, R.; Borrmann, T.; Hoppenheit, R.; Lork, E.; Parsons, S.; Petersen, J.; Schroter, M.; Stohrer, W.-D.; Waterfeld, A.; Watson, P. G. *J. Fluorine Chem.* **2004**, *125*, 1649–1655.
(28) Glemser, O.; Meyer, H.; Haas, A. *Chem. Ber.* **1965**, *98*, 2049–2050.
(29) Glemser, O.; Koch, W. *Z. Naturforsch.* **1968**, *B23*, 745.
(30) Clifford, A. F.; Harman, J. S. *J. Chem. Soc., Dalton Trans.* **1974**, 571–575.
(31) Waterfeld, A.; Bludssus, W.; Mews, R.; Glemser, O. *Z. Anorg. Allg. Chem.* **1980**, *464*, 268–272.
(32) Clifford, A. F.; Howell, J. L.; Wooton, D. L. *J. Fluorine Chem.* **1978**, *11*, 433–439.
(33) Emara, A. A. A.; Schrobilgen, G. J. *J. Chem. Soc., Chem. Commun.* **1987**, 1644–1646.
(34) Emara, A. A. A.; Schrobilgen, G. J. *Inorg. Chem.* **1992**, *31*, 1323–1332.
(35) Schrobilgen, G. J. *J. Chem. Soc., Chem. Commun.* **1988**, 1506–1508.
(36) Emara, A. A. A.; Schrobilgen, G. J. *J. Chem. Soc., Chem. Commun.* **1988**, 257–259.
(37) Fir, B. A.; Whalen, J. M.; Mercier, H. P. A.; Dixon, D. A.; Schrobilgen, G. J. *Inorg. Chem.* **2006**, *45*, 1978–1996.
(38) LeBlond, R. D.; DesMarteau, D. D. *J. Chem. Soc., Chem. Commun.* **1974**, 555–556.
(39) DesMarteau, D. D.; LeBlond, R. D.; Hossain, S. F.; Nothe, D. *J. Am. Chem. Soc.* **1981**, *103*, 7734–7739.
(40) Sawyer, J. F.; Schrobilgen, G. J.; Sutherland, S. J. *Inorg. Chem.* **1982**, *21*, 4064–4072.
(41) Schumacher, G. A.; Schrobilgen, G. J. *Inorg. Chem.* **1983**, *22*, 2178–2183.
(42) Faggiani, R.; Kennepohl, D. K.; Lock, C. J. L.; Schrobilgen, G. J. *Inorg. Chem.* **1986**, *25*, 563–571.
(43) Foropoulos, J. J.; DesMarteau, D. D. *J. Am. Chem. Soc.* **1982**, *104*, 4260–4261.
(44) Beach, D. B.; Jolly, W. L.; Mews, R.; Waterfeld, A. *Inorg. Chem.* **1984**, *23*, 4080–4084.
(45) Smith, G. L.; Mercier, H. P. A.; Schrobilgen, G. J. *Inorg. Chem.* **2007**, *46*, 1369–1378.
(46) Fir, B. A.; Gerken, M.; Pointner, B. E.; Mercier, H. P. A.; Dixon, D. A.; Schrobilgen, G. J. *J. Fluorine Chem.* **2000**, *105*, 159–167.
(47) Fir, B. A. MSc. Thesis, McMaster University, Hamilton, Ontario, Canada, 1999.
(48) Zalkin, A.; Ward, D. L.; Biagioni, R. N.; Templeton, D. H.; Bartlett, N. *Inorg. Chem.* **1978**, *17*, 1318–1322.
(49) Elliott, H. S. A.; Jenkins, H. D. B.; Lehmann, J. F.; Mercier, H. P. A.; Schrobilgen, G. J. *Inorg. Chem.* **2010**, *49*, 8504–8523.
(50) Bartlett, N.; Gennis, M.; Gibler, D. D.; Morrell, B. K.; Zalkin, A. *Inorg. Chem.* **1973**, *12*, 1717–1721.
(51) Gillespie, R. J.; Landa, B. *Inorg. Chem.* **1973**, *12*, 1383–1388.
(52) Gillespie, R. J.; Martin, D.; Schrobilgen, G. J. *J. Chem. Soc., Dalton Trans.* **1980**, 1898–1903.
(53) Buss, B.; Clegg, W.; Hartmann, G.; Jones, P. G.; Mews, R.; Noltemeyer, M.; Sheldrick, G. M. *J. Chem. Soc., Dalton Trans.* **1981**, 61–63.
(54) Behrens, U.; Lork, E.; Petersen, J.; Waterfeld, A.; Mews, R. *Z. Anorg. Allg. Chem.* **1997**, *623*, 1518–1524.
(55) Reed, A. E.; von Schleyer, P. R. *J. Am. Chem. Soc.* **1990**, *112*, 1434–1445.
(56) Smith, G. L.; Schrobilgen, G. J. *Inorg. Chem.* **2009**, *48*, 7714–7728.
(57) Bondi, A. *J. Phys. Chem.* **1964**, *68*, 441–451.
(58) Smith, G. L.; Mercier, H. P. A.; Schrobilgen, G. J. *J. Am. Chem. Soc.* **2009**, *131*, 7272–7286.
(59) DesMarteau, D. D.; Seppelt, K. *Angew. Chem., Int. Ed. Engl.* **1980**, *19*, 643.
(60) DesMarteau, D. D.; Eysel, H. H.; Oberhammer, H.; Günther, H. *Inorg. Chem.* **1982**, *21*, 1607–1616.
(61) Stahl, I.; Mews, R.; Glemser, O. *Angew. Chem., Int. Ed. Engl.* **1980**, *19*, 408–409.
(62) Jameson, C. J. In *Multinuclear NMR*; Mason, J., Ed.; Plenum Press: New York, 1987, Chapter 4, pp 109−110 and references cited therein.
(63) Kleemann, G.; Seppelt, K. *Angew. Chem., Int. Ed. Engl.* **1978**, *7*, 516–518.
(64) Meier, T.; Mews, R. *Angew. Chem., Int. Ed. Engl.* **1985**, *24*, 344–345.
(65) Smith, G. L.; Mercier, H. P. A.; Schrobilgen, G. J. *Inorg. Chem.* **2008**, *47*, 4173–4184.
(66) Reference 37 and references cited therein.
(67) Koppe, K.; Bilir, V.; Frohn, H. J.; Mercier, H. P. A.; Schrobilgen, G. J. *Inorg. Chem.* **2007**, *46*, 9425–9437.
(68) Keller, N.; Schrobilgen, G. J. *Inorg. Chem.* **1981**, *20*, 2118–2129.
(69) Schrobilgen, G. J.; Holloway, J. H.; Granger, P.; Brevard, C. *Inorg. Chem.* **1978**, *17*, 980–987.
(70) Günther, H.; Oberhammer, H.; Mews, R.; Stahl, I. *Inorg. Chem.* **1982**, *21*, 1872–1875.
(71) Mercier, H. P. A.; Moran, M. D.; Sanders, J. C. P.; Schrobilgen, G. J.; Suontamo, R. J. *Inorg. Chem.* **2005**, *44*, 49–60.
(72) Heilemann, W.; Mews, R. *J. Fluorine Chem.* **1988**, *39*, 261–269.
(73) Simon, A.; Peters, E. M.; Lentz, D.; Seppelt, K. *Z. Anorg. Allg. Chem.* **1980**, *468*, 7–14.
(74) Gundersen, G.; Hedberg, K. *J. Chem. Phys.* **1969**, *51*, 2500–2507.
(75) Koppe, K.; Frohn, H.-J.; Mercier, H. P. A.; Schrobilgen, G. J. *Inorg. Chem.* **2008**, *47*, 3205–3217.
(76) Frohn, H.-J.; Jakobs, S.; Henkel, G. *Angew. Chem., Int. Ed. Engl.* **1989**, *28*, 1506–1507.
(77) Frohn, H. J.; Schroer, T.; Henkel, G. *Z. Naturforsch.* **1995**, *50 b*, 1799–1810.
(78) Gibler, D. D.; Adams, C. J.; Fischer, M.; Zalkin, A.; Bartlett, N. *Inorg. Chem.* **1972**, *11*, 2325–2329.

(79) Mallouk, T. E.; Rosenthal, G. R.; Müller, G.; Brusasco, R.; Bartlett, N. *Inorg. Chem.* **1984**, *23*, 3167–3173.
(80) Lehmann, J. F.; Dixon, D. A.; Schrobilgen, G. J. *Inorg. Chem.* **2001**, *40*, 3002–3017.
(81) Turowsky, L.; Seppelt, K. *Inorg. Chem.* **1990**, *29*, 3226–3228.
(82) Frohn, H.-J.; Klose, A.; Schroer, T.; Henkel, G.; Buss, V.; Opitz, D.; Vahrenhorst, R. *Inorg. Chem.* **1998**, *37*, 4884–4890.
(83) Wilson, W. W.; Christe, K. O.; Feng, J.; Bau, R. *Can. J. Chem.* **1989**, *67*, 1898–1901.
(84) Murphy, V. J.; Hascall, T.; Chen, J. Y.; Parkin, G. *J. Am. Chem. Soc.* **1996**, *118*, 7428–7429.
(85) Whittlesey, M. K.; Perutz, R. N.; Greener, B.; Moore, M. H. *Chem. Commun.* **1997**, 187–188.
(86) Brock, D. S.; Bilir, V.; Mercier, H. P. A.; Schrobilgen, G. J. *J. Am. Chem. Soc.* **2007**, *129*, 3598–3611.
(87) Birchall, T.; Myers, R. D.; de Waard, H.; Schrobilgen, G. J. *Inorg. Chem.* **1982**, *21*, 1068–1073.
(88) Boldrini, P.; Gillespie, R. J.; Ireland, P. R.; Schrobilgen, G. J. *Inorg. Chem.* **1974**, *13*, 1690–1694.
(89) Gillespie, R. J.; Landa, B.; Schrobilgen, G. J. *Inorg. Chem.* **1976**, *15*, 1256–1263.
(90) Lehmann, J. F.; Mercier, H. P. A.; Schrobilgen, G. J. *Coord. Chem. Rev.* **2002**, *233*−*234*, 1–39.